# Mag Feet: A Robotic Device for the Inspection of Steel Bridge Structures

by



Anirban Mazumdar

B.S., Mechanical Engineering, Massachusetts Institute of Technology, 2007

Submitted to the Department of Mechanical Engineering in partial fulfillment of the requirements for the degree of

Master of Science in Mechanical Engineering

at the

MASSACHUSETTS INSTITUTE OF TECHNOLOGY

June 2009



Author .....

Department of Mechanical Engineering
May 22, 2009

Certified by .....

H. Harry Asada
Ford Professor of Mechanical Engineering
Thesis Supervisor

Accepted by .....

David E. Hardt
Chairman, Department Committee on Graduate Students
Department of Mechanical Engineering

# Mag Feet: A Robotic Device for the Inspection of Steel Bridge Structures

by

Anirban Mazumdar

Submitted to the Department of Mechanical Engineering
on May 22, 2009, in partial fulfillment of the
requirements for the degree of
Master of Science in Mechanical Engineering

## Abstract

The aging of America's steel bridges presents many challenges. Undetected cracks and corrosion can eventually lead to catastrophic failure. Due to the difficulties with inspecting existing bridges the use of mobile robots for steel bridge inspection has become an important area of research. This thesis describes the analysis, design, and implementation of a new approach to steel bridge inspection robots using tilting feet equipped with permanent magnets. This robot, titled "Mag-Feet", is capable of adhering to steel surfaces and can move along steel surfaces using a combination of three distinct gait modes. These three gait modes allow the robot to "Moonwalk" along horizontal surfaces, "Shuffle" up inclined surfaces, and "Swing" over small obstacles. The "Swing" motions present their own set of interesting challenges. Since the robot can only adhere to the surface using finite (and relatively small) magnetic forces, it may fall due to the reaction forces caused by the swing- up motion. To prevent failure modes, an optimal swing-up trajectory was designed so that the maximum reaction force during the trajectory was minimized. The trajectories were parameterized using sigmoids and were determined by solving the dynamic equations as a 2 point boundary value problem. Finally, a proof of concept prototype was constructed and was used to experimentally evaluate the design. These experiments illustrate the promise of the design and control approaches that were formulated.

Thesis Supervisor: H. Harry Asada
Title: Ford Professor of Mechanical Engineering

# Acknowledgments

First and foremost I would like to thank Professor Asada for his guidance over the past years. His advice, support, and encouragement has been invaluable to me, and I feel like I have made great strides as an engineer, a researcher and as a person under his tutelage. I hope to continue to learn from him in the coming years.

I am also grateful to my colleagues at the D'Arbeloff Laboratory for not only providing me with great insights but also for making the lab environment thoroughly enjoyable and exciting. In particular I would like to thank my good friend Josiah Rosmarin for introducing me to the lab and taking me under his wing. We tend to view the lab as a family, and I feel privileged to be able to work alongside so many bright and interesting men and women.

To my friends I owe many thanks. For my friend Miguel and I this thesis marks the end of a long and eventful journey that began in 2004. We have taken almost every Mechanical Engineering course together and I am sure that I wouldn't be in the position I am today if it was not for his friendship and assistance over the past 5 years. Also I must thank Renee for introducing me to the STEM Program. I have learned so much from my experiences as mentor. Lastly, I would like to my friends who have spent many hours with me at the Rockwell basketball courts. Dyan, Kimi,Yasu, Dan, Kevin, and Vic, I have tremendously enjoyed the time we have spent playing basketball, watching sports, and hanging out. I hope there will be many more such times in the future.

I would also like to thank the National Science Foundation for providing me with the unique opportunity to pursue research as a Graduate Research Fellow. This award has been a great opportunity for me, and I will continue to strive to use my unique position to involve others in science and engineering.

Finally, I must thank my parents for their constant love and encouragement. My parents taught me from a young age about the value of education, and always focused on the importance of using my technical education to benefit my society. I just hope that I can continue to uphold these values in my own life and career.

# Contents

# List of Figures

# List of Tables

# Chapter 1

# Introduction

## 1.1 Inspecting Aging Bridges

As the civil infrastructure of the world ages, time begins to take its toll on these essential structures in the form of corrosion and cracks. Undetected corrosion and cracks can severely compromise the structure and can lead to catastrophic failures that cannot be predicted. Steel structures are especially vulnerable to corrosion, and in the United States of America alone there exist more than 130,000 steel bridges [1].

While there is substantial research in the area of sensor systems such as "smart bridges" with embedded sensors within the structural members [2], these systems are more applicable to new bridges rather than existing and aging ones due to the fact that replacing existing bridge members with "smart ones" is a difficult problem.

In the absences of imbedded monitoring systems, bridges must be inspected periodically. Currently, many bridges are simply inspected visually by workers using temporary scaffolding or other means to reach the underside of bridges. Not only are such inspections time consuming, difficult, and at times dangerous due to the inaccessible nature of many bridge structures, but published reports indicate that factors such as fear of traffic, visual acuity, and accessibility may create variability in the ratings provided by human inspectors [3]. In addition sometimes such inspections involve either shutting down the bridge or limiting access. This introduces additional costs to the inspection process.

## 1.2 A Robotic Solution?

Due to these reasons described above, bridge member inspection is a task where the current advances in mobile robots and robotic technology can be applied. Mobile robots could potentially provide measurements from inaccessible locations and ideally would provide less variable visual measurements while also exposing the inspection teams to less risk and danger. The idea of using robots to provide visual inspections isn't particularly new. For example, [4] recently presented a design for a bridge inspection robot that uses a robotic device mounted on a custom road vehicle to take measurements. Another approach is to use mobile robots that can either grab the steel members or adhere using vacuum forces [5].

Steel bridges offer the potential of using robots that can adhere to the bridge members using magnetic forces. Such mobile robots could potentially carry other sensing devices in addition to cameras. For example, magnetic flux leakage is now a common technique for measuring the level of corrosion or detecting cracks in steel structures.

More specifically, permanent magnets offer substantial promise for the purposes of steel bridge inspection. First, for the force requirements of small mobile robots ($\sim 20N$), rare earth permanent magnets provide a substantially larger strength to weight ratio than electromagnets, which allows for larger payloads. In addition, a robot that uses permanent magnets could hang from steel members without consuming any power. Ideally such robots could loiter on steel members and could provide valuable inspection images or statistics on command.

An obvious extension of this logic is to develop wheeled mobile robots that use permanent magnets. This in fact has been implemented successfully by Professor Alex Slocum at MIT [6]. However, wheeled designs have trouble overcoming obstacles or areas where the magnetic force may be weak. For relatively uncontrolled environments such as bridge members it is important to develop robots that could potentially overcome obstacles.

This thesis describes the design, implementation, and control of a 2 legged robotic

device known as Mag-Feet that uses feet with permanent magnets to adhere to steel surfaces. The robot is underactuated: it uses a single DC motor and two locking mechanisms (one for each leg). The Mag-Feet robot is capable of two modes of sliding locomotion that allows it to move along relatively smooth surfaces. In addition, the robot can overcome small obstacles through the use of a swinging motion that is similar to the brachiation of monkeys. This underactuated swinging problem is solved by parameterizing the trajectory and solving it as a 2 point boundary value problem.

## 1.3 Goals and Organization

This work will focus on the analysis and design of the Mag-Feet robot. Special attention will be paid to the unique "tilting foot" concept. This work will touch on the following areas.

- A description of the functional requirements for a simple bridge inspection robot and a discussion of the mechanical design that resulted.
- An overview of the 3 motion primitives and a discussion of the relevant kinematics and statics
- A discussion of the underactuated swinging problem in the context of generating trajectories that take into account the unique force constraints of the Mag-Feet robot.
- Physical implementation of the mechanical design.
- Experimental evaluation of the solution to the swinging problem.

This work will conclude with an overall discussion of the device and its relative merits and limitations. An outline of future work also be provided.

# Chapter 2

# The Mag-Feet Design

## 2.1 Functional Requirements

For a robot to provide suitable inspection capability there are a number of requirements that must be satisfied. While there is the hope that eventually robotic devices can perform sophisticated non destructive evaluation of bridges, for the time being it makes sense to focus on using robotic devices to perform the visual inspection tasks that are currently in practice. This is similar to the approach taken in [4]. The following requirements exist:

- The ability to carry a small payload that would contain the camera and imaging equipment while adhering to the steel surface.
- The robot must be able to move up and down slightly inclined surfaces
- The robot must be able to deal with small variations in surface geometry and obstacles.

A quick examination of the functional requirements confirms that permanent magnets are a logical starting point due to the fact that rare-earth permanent magnets offer a greater strength to weight ratio than electromagnets for the desired force ranges ($\sim 20N$). In addition, a mobile robot that uses permanent magnets to adhere to the structure requires no input power to hang in place. As described in the introduction,

the third requirement that entails traversing obstacles makes the use of wheels difficult. Therefore it is necessary to explore an alternative to the wheeled locomotion concepts that already exist [6].

## 2.2 The Tilting Foot

One alternative to wheeled locomotion is to use multiple legs. Therefore one leg can be detached and moved around the obstacle while the other leg remains planted on the surface. However, there exists the problem of having to detach a permanent magnet. Unlike electromagnets, the magnet cannot simply be switched off.

One possible solution is to use an actuator at each magnetic foot that can be used to pull the magnet off the surface by acting perpendicular to the surface ($y$ direction) [7]. In this case the detachment force $F_y$ would have to be greater than or equal to the magnetic attachment force $F_m$. Therefore, for larger payloads, larger actuators would be required (which in turn create a heavier robot). In addition, extra actuators tend to increase complexity and power consumption.

The tilting foot is designed to resolve this problem of detachment. Consider a foot that has an edge so that it can rotate about point $B$ (illustrated in Fig. 2-1) when a moment is applied. If $r$ represents the distance from the center of the magnet to this edge, the maximum moment created by the magnetic attachment force about $B$ is approximately $F_m r$. If a horizontal force $F_x$ is applied to the tip of the leg, point $A$, it will generate a moment $F_x h$ about point $B$ on the surface. If this moment is greater than $F_m r$, then the foot will begin to tilt:

$$F_x > \frac{r}{h} F_m \tag{2.1}$$

Note that if the leg length $h$ is much longer than $r$, $F_x$ is significantly smaller than the normal magnet force . As the foot rotates, tilting becomes even easier. This is due to the fact that an air gap is being created between the magnet and the steel surface. $F_m$ decays roughly with the squared distance $d^2$, where $d$ is the air gap.

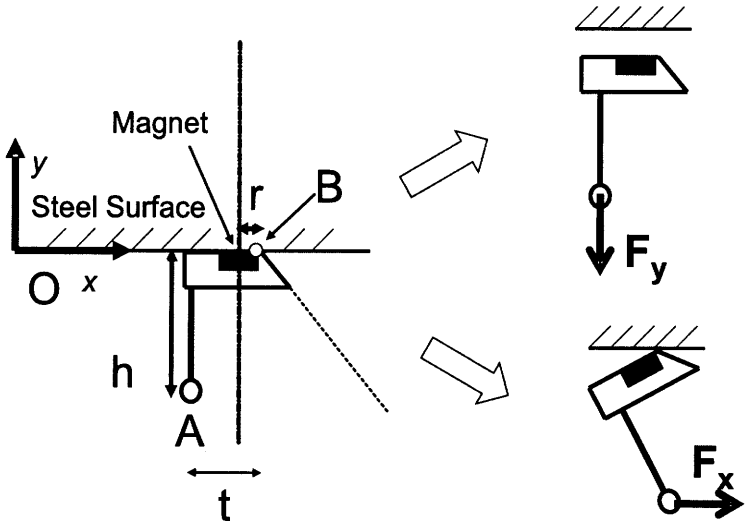


Figure 2-1: A schematic illustration of the foot dimensions and the tilting foot concept. Tilting the specially designed foot requires significantly less force than simply pulling it off of the steel surface. Once the foot is tilted it can be pulled off easily or slid along the surface.

This means that the force $F_y(d)$ needed to detach the foot has now been substantially reduced. In addition, the friction force resisting the sliding motion has been similarly reduced. The tilting of the foot has now greatly eased the actuator requirements for locomotion.

## 2.3 Basic Mechanism Design

The robot mechanism was designed to take full advantage of the tilting foot design and use it for upside-down locomotion along horizontal surfaces and surfaces with small inclines. The robot mechanism was designed for multiple gait modes. The basic mechanism consists of two tilting feet each connected to a leg. The leg joints are connected at a hip joint. Fig. 2-2 illustrates the overall layout of the free ankle joints ($A$) and the hip ($B$) actuated by a rotary actuator. It is important to note that the front edge of the foot is located much closer to the magnet than the rear edge. This means that the horizontal force $F_x$ needed to cause the foot to tilt in the

counter clockwise direction is much lower than the horizontal force $F_x$ required to tilt the foot in the clockwise direction. Notice also that both tilting feet are oriented so that they are pointing in the same direction. This configuration ensures that when a torque is applied between the legs (either pulling them together or pushing them apart), one foot is always much more likely than the other to tilt.

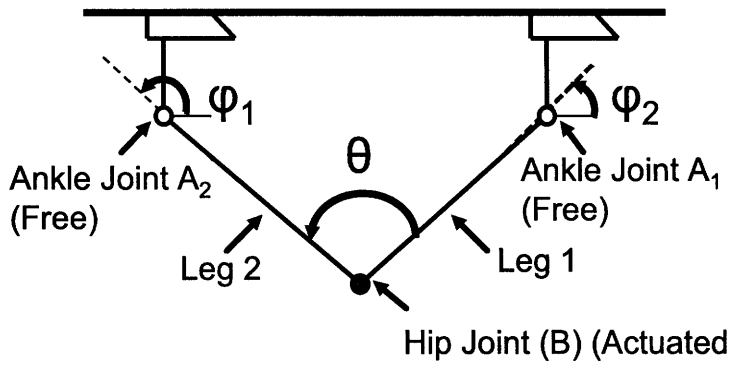


Figure 2-2: A schematic diagram illustrating the basic mechanism design.

## 2.4 Modes of Gait

### 2.4.1 Moonwalk

There exist three basic gait motions that the Mag-Foot robot can achieve. The first gait mode is similar to the way humans slide their feet without lifting them off the ground (similar to a dance move popularized by Michael Jackson), and hence it is named "Moon Walk". As shown in Fig. 2-3, Foot 1 (labeled in black) is fully attached to the steel wall, while Foot 2 (gray) is first tilted in order to reduce the effect of the magnetic force, and then pulled along the surface, so it slides on it. After passing Foot 1, Foot 2 is stopped at an appropriate distance, and is rotated backwards, so that it can fully engage with the steel surface. The process is repeated as gait proceeds.

Note that, when Foot 2 passes Foot 1, joints $A_1$ and $A_2$ momentarily come to the same location. As will be discussed later in detail, an undesired behavior may occur at this particular configuration, since legs 1 and 2 together can freely rotate about joint $A_1$ ($A_2$). It is a type of singularity.

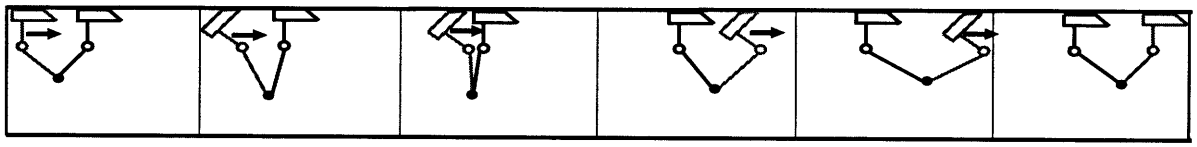

Figure 2-3: An illustration of the moonwalk gait. The planted foot is labeled in black while the moving foot is labeled in gray.

### 2.4.2 Shuffle

To prevent this singular configuration from occurring, we propose another gait mode, called the "Shuffle". The shuffle gait mode is the same as the Moon-Walker mode except that the stride is less than a half of the latter, so that Foot 2 does not pass Foot 1. This mode of gait is illustrated in Fig. 2-4.

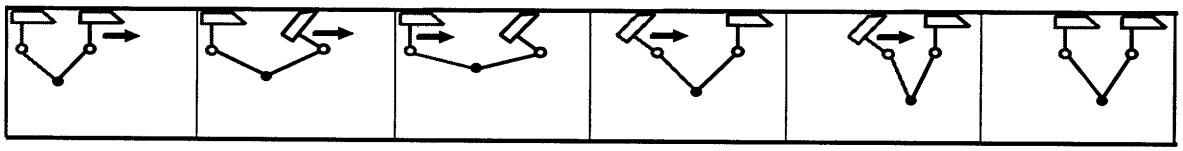

Figure 2-4: An illustration of the shuffle gait. The planted foot is labeled in black while the moving foot is labeled in gray.

### 2.4.3 Swing

The third gait mode is called "Swing." The swing mode consists of first tilting Foot 1 in order to reduce the magnetic force. The ankle joint $A_1$ is then locked (note the change in color to blue). Foot 1 is then detached completely from the steel surface and swung around. This mode is useful for traversing obstacles and is illustrated in Fig. 2-5.

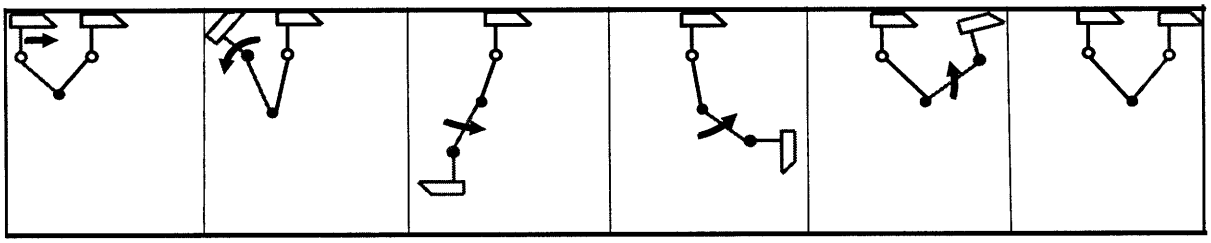

Figure 2-5: An illustration of the swinging gait. The planted foot is labeled in black while the moving foot is labeled in gray.

# Chapter 3

# Kinematic and Static Analysis

## 3.1 Motion Primitive Kinematics

The motions that comprise the 3 gait modes can be divided into 3 motion primitives. These primitives are tilting, sliding, and swinging. This section will discuss the relevant kinematics for each motion primitive.

### 3.1.1 Foot Tilting

The most important and prevalent motion primitive is foot tilting. Foot tilting consists of rotating the foot about point $B$ in Fig. 3-1). This foot tilting is required for all the three gait modes. As shown in Fig. 3-1), the rotating foot, the two legs, and the fixture form a four-bar linkage. Let $\beta$ be the angle of foot rotation about point $B$. There exists a functional relationship between the hip angle $\beta$ and this foot rotation angle. This result is provided in equations 3.1 to 3.3.

$$\cos\eta = \frac{r_{tilt}^2 + h^2 + x_{tilt}^2 + 2L_1^2\cos\theta - 2L_1^2}{2r_{tilt}\left(h^2 + r_{tilt}^2\right)^{\frac{1}{2}}} \tag{3.1}$$

$$\tan\delta = \frac{h}{x_{tilt}} \tag{3.2}$$

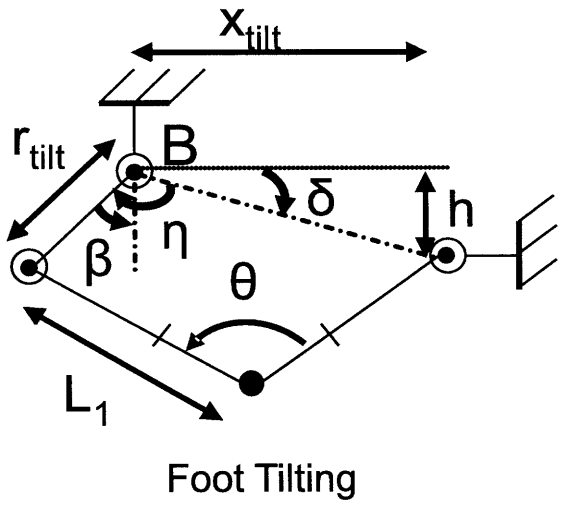


Figure 3-1: A diagram illustrating the tilting primitive.

$$\beta = \delta + \eta - \frac{\pi}{2} \tag{3.3}$$

### 3.1.2 Foot Sliding

Following the tilting motion, the foot must be moved along the surface. This sliding primitive, too, is involved in all three gait modes. We assume that the tilting edge is completely aligned to the surface making a surface-to-surface contact. Under this assumption, the foot sliding can be modeled as another four-bar-linkage with three revolute joints and one prismatic joint Fig. 3-2). If we recall that the leg length is $L_1$ for both legs, the relationship between the step size ($x_{slide}$) and the hip angle $\theta$ is provided in equation 3.4.

$$x_{slide} = 2L_1 \sin\frac{\theta}{2} \tag{3.4}$$

### 3.1.3 Foot Swinging

The swinging mode introduces a new set of independent generalized coordinates for describing the kinematics. Since the rear foot is assumed to be locked, the rear leg

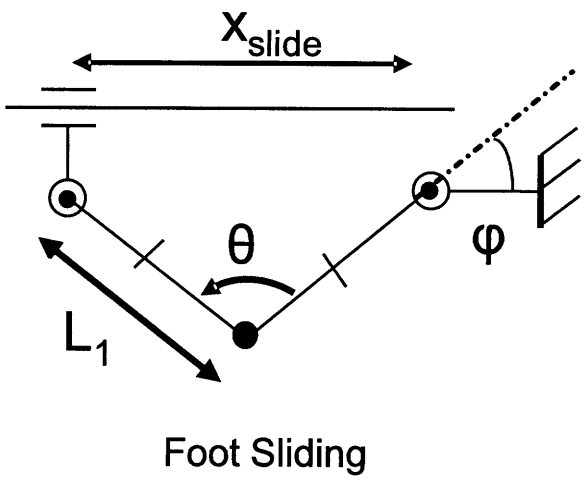


Figure 3-2: A diagram illustrating the sliding primitive.

and foot can be drawn as a single rigid body of length ($L_{lock}$) with angle $\alpha$ with respect to the front leg. Now both the ankle angle $\phi$ and this new hip angle $\alpha$ are required to determine the position of the tilted foot $(x_{swing}, y_{swing})$.

$$\begin{bmatrix} x_{swing}(\alpha, \phi) \\ y_{swing}(\alpha, \phi) \end{bmatrix} = \begin{bmatrix} -L_1 \cos\phi + L_{lock} \cos(\alpha + \phi) \\ -L_1 \sin\phi + L_{lock} \sin(\alpha + \phi) \end{bmatrix} \tag{3.5}$$

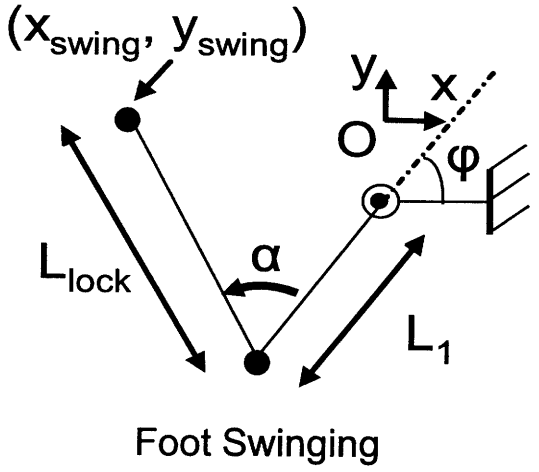


Figure 3-3: A diagram illustrating the swinging primitive.

### 3.1.4 Singularity Analysis

Kinematic analysis reveals the presence of a type of singularity at $\theta = 0$ for the sliding mode. Since during the sliding mode, Leg 1 and Leg 2 are of equal length ($L_1$), the ankle joints ($\phi_1, \phi_2$) are equal when $\theta = 0$. Therefore the following relationship exists between the common ankle joint value angle ($\phi$) and the hip angle ($\theta$).

$$\sin\theta = \sin\varphi_1 \cos\varphi_1 \pm \sin\varphi_1 \cos\varphi_1 \tag{3.6}$$

$$\sin\theta = \begin{cases} 2\sin\varphi_1 cos\varphi_1 \\ 0 \end{cases} \tag{3.7}$$

From these equations it is clear that the kinematic relationship between $\phi$ and $\theta$ breaks down at $\theta = 0$ indicating the presence of a kind of singularity [8]. At this configuration, the ankle angles ($\phi_1, \phi_2$) are no longer defined by the mechanism. This is especially problematic in light of the fact that the Mag-Foot robot is intended to walk on inclined surfaces. Gravity can act on the mechanism and cause its configuration to change. This change in configuration means that the sliding mode kinematics (described above) no longer accurately describes the system. This problem necessitated the development of the "Shuffle" gait mode described in Section 2.4. This gait allows the Mag-Foot robot to walk along surfaces without passing through the singularity. This mode should prove especially useful for locomotion along inclined surfaces where gravity can act to disturb the mechanism. While under idealized conditions, the mechanism gains the additional degree of freedom at exactly $\theta = 0$, this assumes that there is no play in the joints. Should play exist in the joints, deviations from the normal kinematics can occur in the vicinity of $\theta = 0$. This is best illustrated in Fig. 3-4 which reveals the joint space motions for differing amounts of play in the ankle joints. What is clear from this diagram is that for any finite amount of play there exists a clear tendency of the mechanism to deviate from the sliding mode kinematics (labeled in black) as it passes the singularity. A potential solution is to maximize momentum when passing through the singularity. If the momentum of the

hip mass is high it is less likely to deviate from its path. This could be instituted using a "Bang-Bang" type of control approach that causes the foot to slide as fast as the actuator can move it.

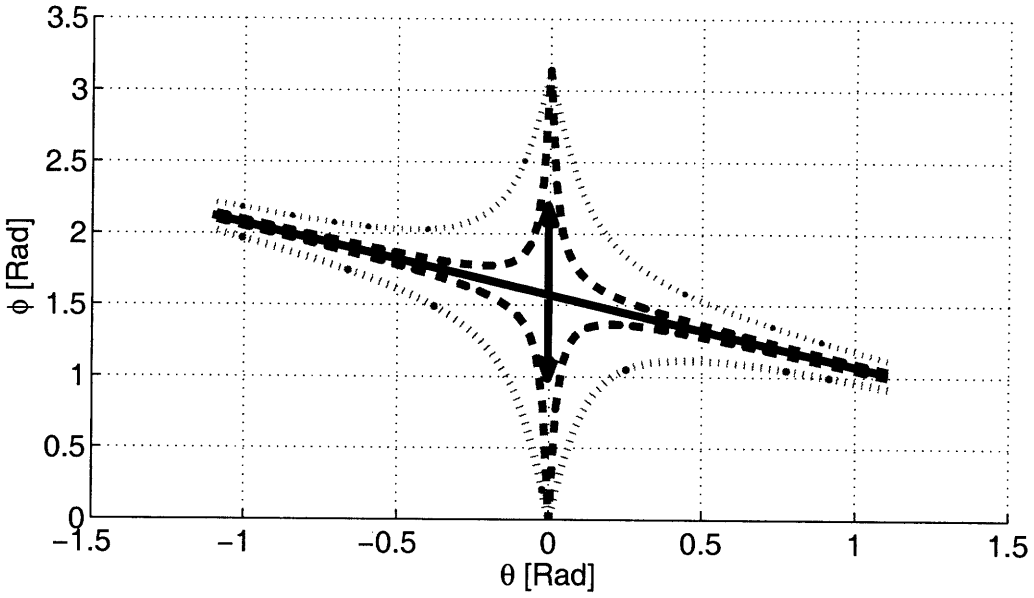


Figure 3-4: A joint space plot of the mechanism configuration as it passes through the singularity. It illustrates the tendency of the mechanism to deviate from the sliding mode kinematics (black line) as the singular configuration is approached

## 3.2 Static Analysis

In the above kinematic analysis using the equivalent kinematic models we assumed that all revolute and prismatic joints do not disjoint. In reality, magnetic feet may be detached from the surface, since they are held by magnetic forces, not by structures. We have to assure that at least one foot remains completely fixed while the other moves. Should this "planted" foot fail to remain fixed, the robot is likely to fall. For the other foot, too, it must not lose contact with the surface while it is rotating or sliding. Furthermore, to perform Swinging mode gait one foot must be detached in the face of the magnetic force. All of these require force and moment analysis so that conditions can be found that guarantee each of the motion primitives to be performed properly. Throughout this section Foot 1 will refer to the planted foot while Foot

2 will describe the foot that is undergoing either tilting, sliding, or detachment / swinging.

### 3.2.1 Foot Tilting

The analysis in this section is only valid if the foot tilts before sliding. If this condition is satisfied, we can perform simple static analysis. Static analysis on the robot mechanism provides the motor torque ($\tau_{tilt}$) requirements for making the foot tilt. Note that $m_1$ represents the total mass of the hip assembly, $\mu_{s,i}$ represents the static coefficient of friction between Foot i (either 1 or 2) and the surface, and $F_m(d)$ represents the magnetic clamping force as a function of the air gap $d$. Also recall that $r$ represents the distance from the center of the magnet to the tilting edge of the foot, and $t$ represents the x distance from the tilting edge to the ankle. The torque needed for tilting the foot is summarized in eq. 3.8.

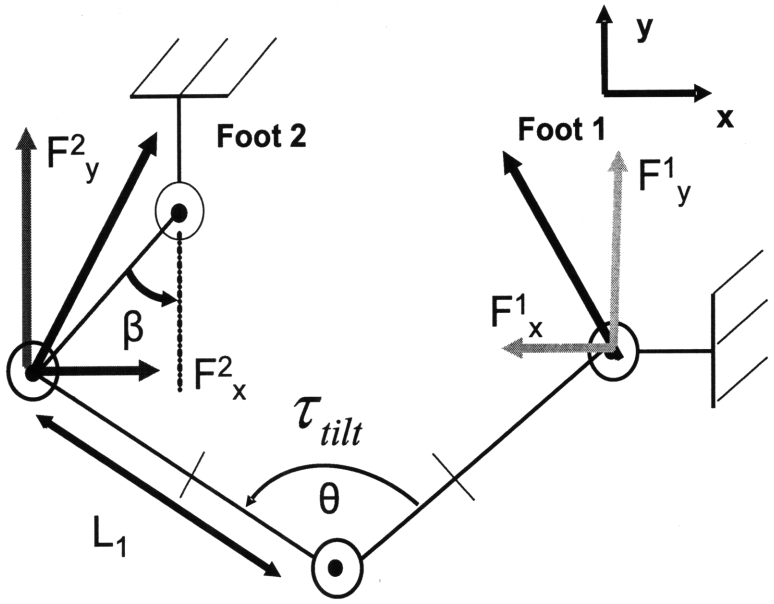


Figure 3-5: A figure illustrating the forces on the tilting foot (Foot2) and the planted foot (Foot1) during a tilting motion.

$$\tau_{tilt} = L_1 \frac{F_m(d=0)r - \frac{m_1 g}{2}(t + h\tan(\frac{\theta}{2}))}{t\sin(\frac{\theta}{2}) - h\cos(\frac{\theta}{2})} \tag{3.8}$$

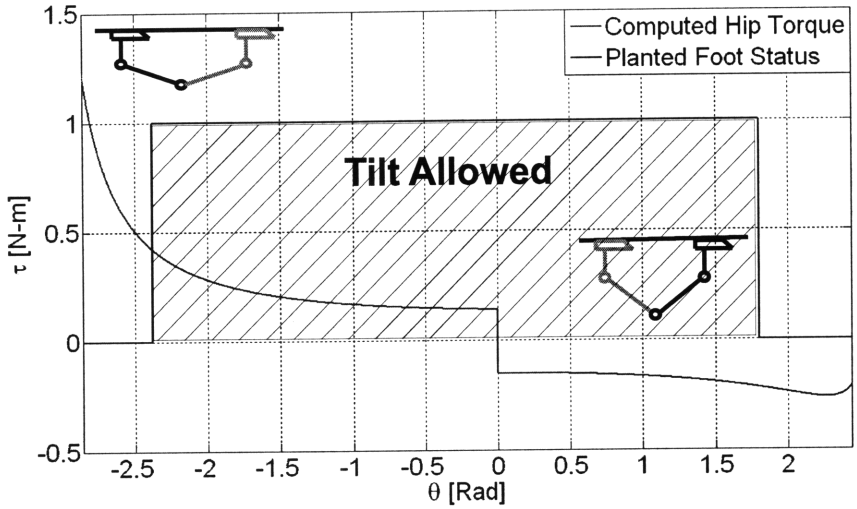


Figure 3-6: A plot illustrating the torque ($\tau_{tilt}$) required to tilt the foot based on the hip angle ($\theta$). Note the presence of zones where tilting will cause the planted foot to detach and the mechanism to fail. The cartoons provide visual illustrations of some allowable and dangerous initial configurations. Note that the grayed out foot and leg is the one to be tilted.

Note that the worst case scenario is $d = 0$ (no air gap means highest magnetic force) therefore, this will be used for determining actuator specifications. A key concern with this design is that the feet follow the desired motions. Specifically, the "planted foot" must not slide or detach while the other foot is being tilted. In addition, the tilting foot must tilt in the correct direction. The above analysis can be used in combination with basic static analysis on the mechanism to determine at which configurations the mechanism will fail. The goal is to determine at what configurations the planted foot will no longer remain planted. Specifically, we can examine the reaction forces $F_x^1$ and $F_y^1$ on Foot 1. Foot 1 will detach if the constraint outlined in eq. 3.9 is violated.

$$F_y^1 < -F_m(d = 0) \tag{3.9}$$

Note that the distance $d$ is set to zero because Foot 1 is assumed to be planted. The results of this static analysis are provided in Fig. 3-6. Fig. 3-6 plots the required

hip torque ($\tau_{tilt}$) versus the hip angle. This plot reveals that there exist certain $\theta$ values that cause the planted foot to detach. The planted foot "status" is plotted as a boolean value. If the foot detaches, the foot status is plotted as false (0). This result provides important insights into the design because it illustrates that tilting cannot occur at certain configurations that therefore must be avoided.

### 3.2.2 The Importance of Friction

The "tilt before sliding" is based on the existence of a friction force between the foot and the surface. If the surfaces in question are slippery and do not provide sufficient friction, problems can arise. For example if the constraint in eq. 3.10 is violated at Foot 2, the foot will tend to slide in the positive $x$ direction rather than tilting. Similarly, if the condition is violated for Foot 1, the planted foot will slide backwards.

$$\mu_{s,1}, \mu_{s,2} > \frac{r}{h} \tag{3.10}$$

### 3.2.3 Sliding

Similarly, static analysis can be used to determine the sliding torque ($\tau_{slide}$). A key assumption here is that the foot tilts completely so that the edge of the foot is now parallel with the steel surface. This is essential for the sliding mode kinematics. Using the same assumptions as those outlined above, the torque necessary to slide the foot from rest along a surface with static friction coefficient $\mu_s$ can be computed. Note that the normal force between the foot and the surface is again approximated as $F_m(d)$ (the clamping force of the magnet). The result is provided in eq. 3.11.

$$\tau_{slide} = l_1[\frac{m_1 g}{2}\sin\frac{\theta}{2} - F_m(d = d_{slide})\frac{r}{h}\cos\frac{\theta}{2}] \tag{3.11}$$

Note that the air gap d is now set to $d_{slide}$. Since $d_{slide}$ is greater than zero, the torque contribution from the magnetic force is reduced substantially. A negative

torque causes the foot to slide in the positive x direction. This is a result of the use of a right handed coordinate system. Note that now a large friction coefficient $\mu_s$ is not desirable. This requirement must be reconciled with the need for sufficient friction to allow tilting (discussed in section 3.2.1). One obvious way to reconcile these conflicting requirements is to design the planted edge of the foot to have a much larger coefficient of friction than the sliding edge. This can be done by varying the surface finish or through the use of different materials. This approach would have the added benefit of reducing the likelihood of marring the surface during sliding.

### 3.2.4 Detachment

The torque necessary to detach the foot from the surface must also be considered. For detachment, the ankle joint must be locked so the angle between Foot 2 and the leg is fixed. Following an approach similar to that for the tilting case, free body diagrams were used to determine the forces on the mechanism as a result of the detachment torque. Since tilting angles are small, it was assumed that the pseudo hip angle ($\alpha$) was approximately equal to the actual hip angle $\theta$ (in reality they are within 4 degrees of each other). The estimate for the detachment torque is provided in eq. 3.12.

$$\tau_{slide} = L_{lock} \frac{F_m(d) - \frac{m_1 g}{2}}{\sin \frac{\theta}{2}} \tag{3.12}$$

Note that the detachment torque can potentially cause Foot 2 to either tilt or detach. The tendency to tilt is especially dangerous because the tilting foot is designed so that it will tilt with low positive horizontal forces ($F_x^1$). The results of this static analysis are provided in Fig. 3-8 which plots the required detachment torque ($\tau_{detach}$) versus hip angle ($\theta$). The planted foot "status" is plotted as a boolean value on the same axis. If the foot slides or detaches, the foot status is plotted as false (0).

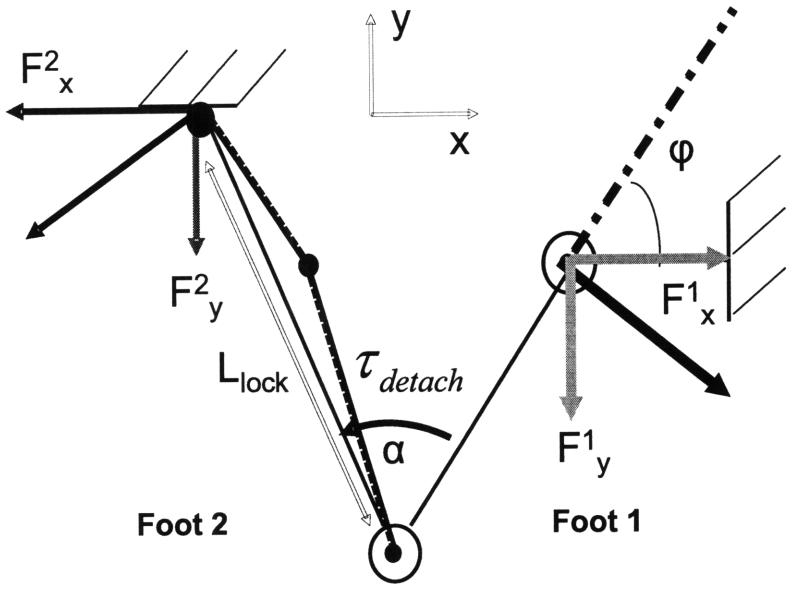


Figure 3-7: A figure illustrating the forces on the tilting foot (Foot2) and the planted foot (Foot1) during a detaching motion.

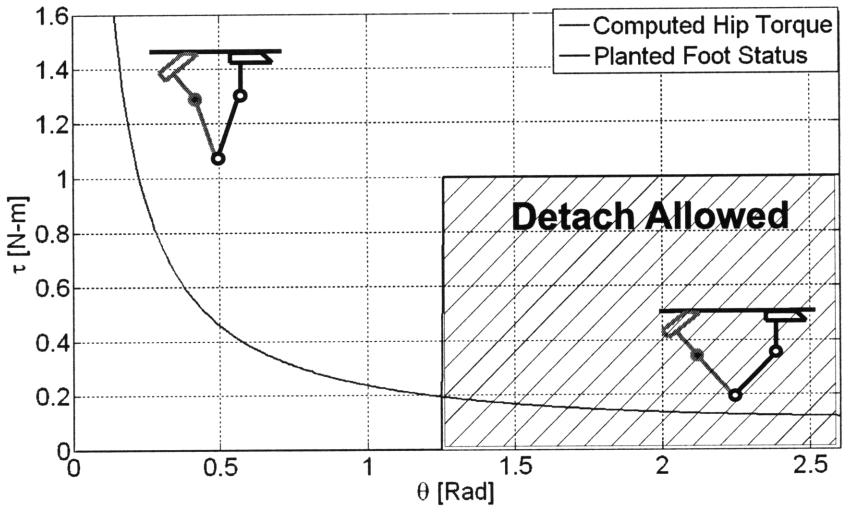


Figure 3-8: A plot illustrating the torque ($\tau_{detach}$) required to detach the foot based on the hip angle ($\theta$). Note that below a certain value $\theta$, detachment torques will cause the planted foot to fail. The cartoons provide visual illustrations of some allowable and dangerous initial configurations. Note that the grayed out foot and leg is the one to be detached.

## 3.3 Comments on the Design

Note that this design provides no actuation on the ankle joints. This lack of actuation creates some concerns when it comes to dealing with singularities (these concerns are addressed through the use of the "shuffle gait mode". However, it should be noted that for ceiling robots, minimizing weight is a crucial issue. Using an underactuated design reduces both weight and mechanical complexity.

As is illustrated in this chapter, the sliding and tilting primitives are 1 DOF motions where the configuration is completely defined by the hip angle. Therefore additional actuators at the ankle would either have to be backdriveable, or they would have to be coordinated perfectly with the hip angle. This would add additional complexity to the control of the device.

In addition, for underactuated swinging motions, the ankle actuator would have to be easily backdriveable in order to minimize dissipation of energy. An obvious alternative would be to not use underactuated swinging motions but instead use the hip and ankle actuators to servo the mechanism in 2D. This, however, would require substantial torques at the ankle necessitating a large actuator or a gearing mechanism.

There is no doubt that additional actuation at the ankles would increase the applicability of the device beyond horizontal ceiling surfaces while also greatly simplifying the swinging controls problem. Therefore additional actuation remains an exciting area for future exploration. However, in the case of inspecting ceiling surfaces that are relatively horizontal, the use of an underactuated scheme is the approach that we feel best reduces weight, mechanical complexity, and coordination.

# Chapter 4

# The Swinging Problem

## 4.1 Introduction

The goal of the swinging gait mode was to allow the robot to successfully traverse small obstacles or areas where the magnetic attachment force would be weak. While the starting point is determined by the nature of the mechanism, there exists a need to choose the correct the landing point in order to safely avoid obstacles of differing size. This has been termed the "irregular ladder problem".

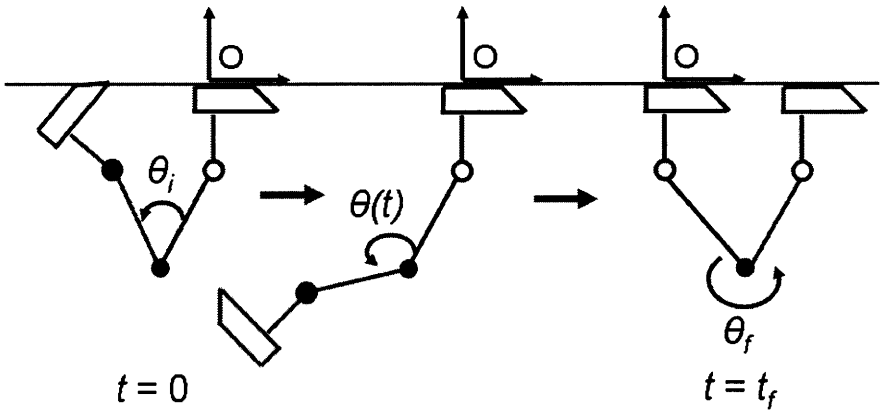


Figure 4-1: An illustration of the rigid body model used for the swinging dynamics.

The study of developing swinging trajectories for such underactuated robots is

not new. Numerous methods for swing up control of similarly underactuated robots have been proposed and evaluated in [9], [10]. In addition, an extensive study of the irregular ladder problem was performed in [11].

However, these previous works involved using a robot with a fairly strong gripping mechanism for holding on during the swinging motions. Therefore, this previous work did not have to consider the reaction forces incurred at the gripper. In contrast, the Mag-Feet robot adheres to the surface using finite magnetic forces. If these forces are exceeded during a swinging motion, the robot will likely detach from the surface, leading to catastrophic failure.

A simple study of the model based approach used in [11] implies that there will be trajectories that violate the constraints on the Mag-Feet robot. As a result there exists a need for a set of trajectories that could be expected to allow the Mag-Feet robot to swing along a surface without falling off. This chapter will focus on the development and analysis of a new set of trajectories that will allow the Mag-Foot robot to solve the irregular ladder problem while satisfying the force constraints unique to this type of robot.

## 4.2 Failure Prevention

As Fig. 4-2 illustrates, swinging motions will result in reaction forces at the planted foot. These forces can cause the failure of the planted foot through detachment or tilting. Specifically, the equations 4.1 to 4.3 outline the criteria for preventing the failure of the planted foot. Recall that $r$ represents the distance from the tilting edge to the center of the magnet, $w$ represents the distance from the center of the magnet to the rear edge of the foot, $d$ represents that air gap between the magnet and surface, and $h$ represents the height at which the forces are applied (see Fig. 4-3).

$$F_y^A > -F_m(d = 0) \tag{4.1}$$

$$F_x^A > -F_m(d=0)\frac{w}{h} \tag{4.2}$$

$$F_x^A < F_m(d=0)\frac{r}{h} \tag{4.3}$$

Throughout any swinging motion, these constraints must be satisfied to ensure that no failure occurs. Note that since $h >> r$, and $w \sim 3r$, the third constraint is the most restrictive. This is logical because the tilting foot was designed specifically to tilt when a small force is applied in the positive $x$ direction.

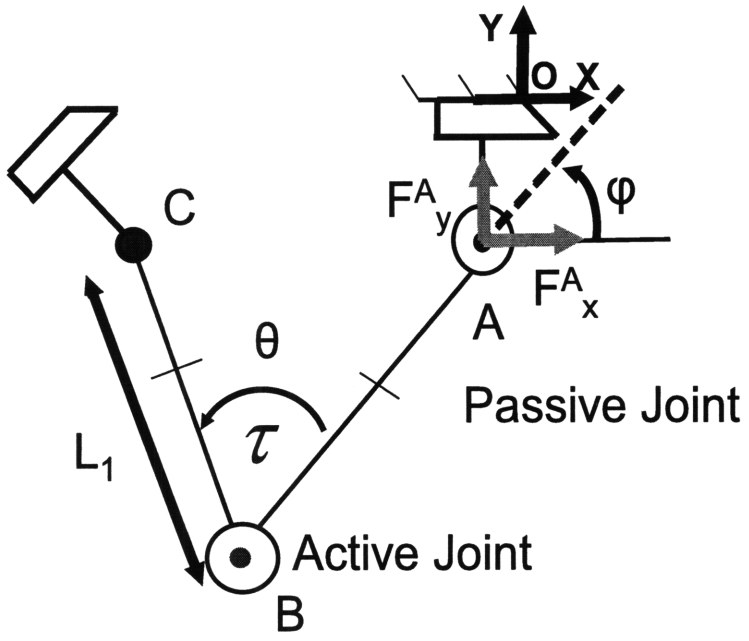


Figure 4-2: An illustration of the rigid body model used for the swinging dynamics.

## 4.3 System Model

A simplified rigid body model is used to approximate the system. Since the mass of the system is concentrated near the hip joint (due to the motor) and the ankle (due to the locking mechanism), the model simply assumes that there are point masses at points $A$, $B$, and $C$ ($m_A$, $m_B$, $m_C$). The masses of the links are small compared to

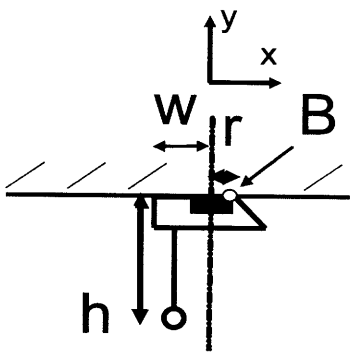


Figure 4-3: An illustration of the tilting foot geometry.

these masses and are therefore approximated as massless links.

The hip angle ($\theta$) and the ankle angle ($\phi$) are used as the generalized independent coordinates, and the resulting dynamic equations are of the form in eq. 4.4.

$$\begin{bmatrix} \tau \\ 0 \end{bmatrix} - \begin{bmatrix} b_\theta & 0 \\ 0 & b_\phi \end{bmatrix} \begin{bmatrix} \dot{\theta} \\ \dot{\phi} \end{bmatrix} = H(\theta,\phi) \begin{bmatrix} \ddot{\theta} \\ \ddot{\phi} \end{bmatrix} + C(\theta,\phi,\dot{\theta},\dot{\phi}) \begin{bmatrix} \ddot{\theta} \\ \ddot{\phi} \end{bmatrix} + G(\theta,\phi) \quad (4.4)$$

In eq. 4.4 $H$ represents the inertia matrix, $C$ represents the Coriolis terms, and $G$ represents the gravitational terms. In addition, $b_\theta$ and $b_\phi$ represent the viscous damping at each joint.

$$H = \begin{bmatrix} m_C L_1^2 & m_C L_1^2 - m_C L_1^2 \cos\theta \\ m_C L_1^2 - m_C L_1^2 \cos\theta & m_B L_1^2 + 2 m_C L_1^2 (1 - \cos\theta) \end{bmatrix} \quad (4.5)$$

$$C = \begin{bmatrix} m_C L_1^2 \dot{\phi} \sin\phi & -m_C L_1^2 \dot{\phi} \sin\phi \\ 2 m_C L_1^2 \dot{\phi} \sin\phi + m_C L_1^2 \dot{\theta} \sin\theta & m_C L_1^2 \dot{\phi} \sin\phi \end{bmatrix} \quad (4.6)$$

$$G = \begin{bmatrix} m_C L_1 g \cos(\phi + \theta) \\ -(m_B + m_C) g L_1 \cos\phi + m_C L_1 g \cos(\phi + \theta) \end{bmatrix} \quad (4.7)$$

This dynamic model can also be used to calculate the reaction forces exerted on the planted foot by the system $(F_x^A, F_y^A)$.

$$F_x^A = -(m_B \ddot{x_B} + m_C \ddot{x_C}) \tag{4.8}$$

$$F_y^A = -(m_B \ddot{y_B} + m_C \ddot{y_C}) - (m_B + m_C)g \tag{4.9}$$

The accelerations $(\ddot{x_B}, \ddot{y_B}, \ddot{x_C}, \ddot{y_C})$ can be determined using the kinematics of the mechanism.

$$\ddot{x_B} = L_1 \ddot{\phi} \sin\phi + L_1 \dot{\phi}^2 \cos\phi \tag{4.10}$$

$$\ddot{y_B} = -L_1 \ddot{\phi} \cos\phi + L_1 \dot{\phi}^2 \sin\phi \tag{4.11}$$

$$\ddot{x_C} = L_1 \ddot{\phi} \sin\phi + L_1 \dot{\phi}^2 \cos\phi + -L_1(\ddot{\phi} + \ddot{\theta}) \sin(\phi + \theta) - L_1(\dot{\phi} + \dot{\theta})^2 \cos(\phi + \theta) \tag{4.12}$$

$$\ddot{y_C} = -L_1 \ddot{\phi} \cos\phi + L_1 \dot{\phi}^2 \sin\phi + L_1(\ddot{\phi} + \ddot{\theta}) \cos(\phi + \theta) - L_1(\dot{\phi} + \dot{\theta})^2 \sin(\phi + \theta) \tag{4.13}$$

## 4.4 An Optimization Problem

As previously described, we desire to swing from an initial configuration $\theta_i$ to a set of final configurations $\theta_f$ without violating our 3 force constraints outlined above. Our problem is essentially a trajectory generation problem; we would like to generate the trajectory that allows us to swing between 2 points while also preventing the robot from falling off. One approach is to examine our trajectory generation problem through the framework of Optimal Control. In this case our cost function should relate to the restrictive force constraint (eq. 4.3). From this this point we will refer to this constraint as the "no tilt constraint".

Formulating the cost function is perhaps the most important step in solving an optimal control problem. It is intuitive to suggest minimizing the reaction force $F_x^A$ as this is likely to prevent violation of the no tilt constraint. However, it should be noted that at no point during the trajectory can the no tilt constraint be violated. Even if the constraint is violated only for a small amount of time the robot is likely to fail. Therefore it is appropriate to formulate a minimax cost function. Specifically, we would like to find the optimal input trajectory $u^*(t)$ that has the smallest peak reaction force $F_x^A$.

$$u^*(t) = \arg\min_{u(t)} \{ \max_{0<t<t_f} [F_x^A(t)] \} \tag{4.14}$$

This idea is illustrated visually below. We desire to minimize the size of the peak reaction force (circled in red). Note how in this case the peak reaction force actually exceeds the no tilt constraint and would therefore lead to failure. It is important to use trajectory generation to make this peak as small as possible.

The problem of dealing with large reaction forces is not new. For example [12] did studies on developing time optimal trajectories with force constraints for a manipulator mounted on a moving tank-like platform where large forces would cause the base to tip or fall. Similarly, [13] studied minimizing reaction forces and torques of a manipulator mounted on a suspended platform. One interesting problem that is similar to our swinging problem is the problem of a manipulator mounted on a spacecraft. Large reaction forces will cause the spacecraft to move, and while jets can be used to counter these forces, minimizing the reaction forces will reduce fuel consumption [14]. In [13] and [14] they minimize reaction forces by exploiting the kinematic redundancy of their manipulator. This approach while valuable and effective cannot be applied to our problem due to the fact that we have an underactuated system that is subject to gravitational forces. In addition, unlike the problem explored in [12] we wish to develop trajectories that minimize the reaction force rather than simply constrain it. This is preferable because there could be cases where our force constraints change (such as inspecting different types of surfaces).

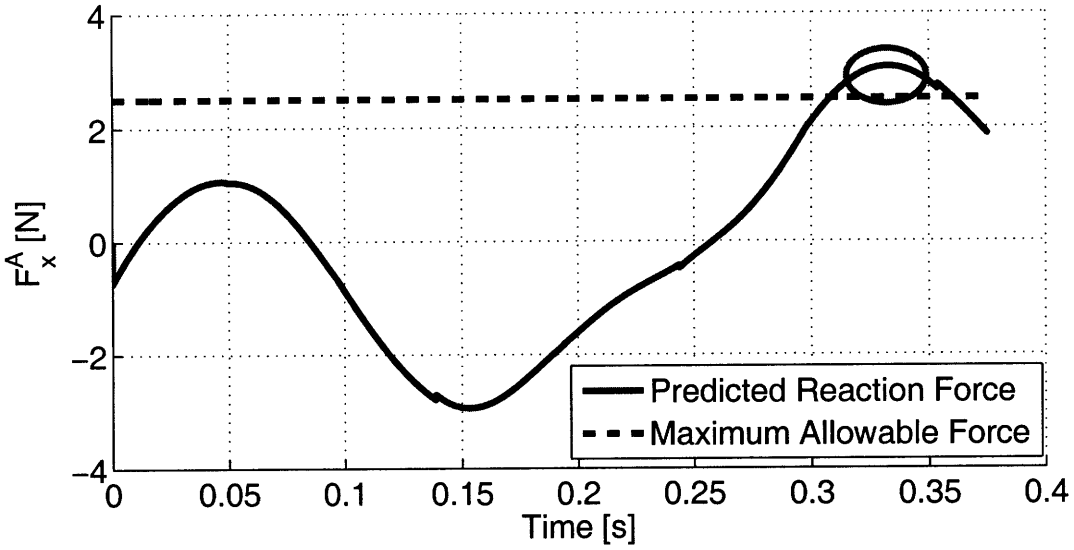


Figure 4-4: An illustration of the described optimization. The goal is to choose a trajectory that best minimizes the peak reaction force (circled in red).

### 4.4.1 State Equations

We can use the dynamic equations outlined in Section 4.3 to produce the dynamic state equations. Note that for the Optimal control formulation we neglect the viscous damping in the joint by assuming that these losses are very small.

$$X = \begin{bmatrix} \theta \\ \phi \\ \dot{\theta} \\ \dot{\theta} \end{bmatrix} \tag{4.15}$$

$$\dot{X} = \begin{bmatrix} 0 & 0 & 1 & 0 \\ 0 & 0 & 0 & 1 \\ 0 & 0 & -(H^{-1}C)_{11} & -(H^{-1}C)_{12} \\ 0 & 0 & -(H^{-1}C)_{21} & -(H^{-1}C)_{22} \end{bmatrix} X - \begin{bmatrix} 0 \\ 0 \\ (H^{-1}G)_1 \\ (H^{-1}G)_2 \end{bmatrix} + \begin{bmatrix} 0 \\ 0 \\ (H^{-1})_{11} \\ (H^{-1})_{21} \end{bmatrix} \tau \tag{4.16}$$

### 4.4.2 Boundary Conditions

The boundary conditions are listed in eq. 4.17 and 4.18. Note that the robot starts and ends with net zero velocity. The landing velocity is especially important, because "hard landings" can damage the mechanism and the steel surface (hardly ideal for an inspection robot). Also it is important to note that the statics of the system impose a single starting configuration $(\theta_i, \phi_i)$. Therefore while we solve the swinging problem for a variety of landing configurations we will use just one initial configuration.

$$X(t=0) = \begin{bmatrix} \theta_i \\ \phi_i \\ 0 \\ 0 \end{bmatrix} \tag{4.17}$$

$$X(t=t_f) = \begin{bmatrix} \theta_f \\ \phi_f \\ 0 \\ 0 \end{bmatrix} \tag{4.18}$$

Since the stated goal is to develop trajectories that minimize a certain cost function, an obvious approach is to solve the problem using the well developed Optimal Control techniques to formulate the problem as a boundary value problem. However, due to the dynamics of the system, the landing time $t_f$ cannot simply be imposed arbitrarily on the system. For example could be landing times at which there will be no viable trajectory for a specified landing time. In most applications, the landing time $(t_f)$ does not have to be very specific. However, for implementation it makes sense to place a limit on $t_f$ to limit the search space, and due to the fact that there will be dissipative forces that will remove energy from the system over time. Therefore, the nature of this problem does not lend itself to the typical Optimal Control solution which involves using the calculus of variations to first formulate and then solve a boundary value problem. Instead, it is a type of "unspecified terminal time problem" which are typically difficult to solve analytically [15].

### 4.4.3 Solving the Optimal Control Problem

Solving the Optimal Control Problem as formulated above is difficult for a number of reasons. First, the unspecified terminal time makes solving it as a two point boundary value problem very difficult. Instead we choose to solve the problem numerically. There exist several commercial Matlab packages that are designed to solve difficult Optimal Control problems such as PROPT, RIOTS, DIRECT, GPOPS, and DIDO. The DIDO package was chosen due to its relative availability, compatibility with recent versions of Matlab, and due to its ability to solve unspecified terminal time problems. The DIDO program uses an adaptive spectral algorithm based on pseudospectral approximation theory [16]. The solutions generated by this problem are referred to "Pseudo-Optimal Results" due to the fact that the program is not given the necessary conditions of optimality. However, the intention was not to find the absolute best trajectory but a set of trajectories that did a sufficiently good job of ensuring that the reaction force in the x direction did not violate the set of constraints. At the very least, such "Pseudo Optimal" results can provide insights into the general shape of the optimal trajectory.

Another problem that arises is that the minimax cost function (eq. 4.14) is not tailored specifically for the typical optimal control formulation which uses an integral cost function. In fact, the DIDO problem had difficulties with the minimax formulation itself. We can convert our cost function into the standard Bolza form using the technique outlined in [17].

$$max(h(t)) = \lim_{q \to \infty} \{ \int_0^{t_f} [h(t)]^q dt \}^{\frac{1}{q}} \tag{4.19}$$

Using this property we can now formulate our cost function to minimize ($J$) in the Bolza form.

$$J = \int_0^{t_f} [F_x^A(t)^2]^q \tag{4.20}$$

Where $q$ is a large positive integer ($q \sim 5$). In addition, several constraints were included to take into account factors that affect the real system. First, the actuator torque was bounded to match the torque capabilities of commercial DC Motors. In addition, constraints were added for the hip angle $\theta(t)$ in order to ensure that the foot would properly detach. A simple way to do this was to place a lower bound on $\theta(t)$.

### 4.4.4 Pseudo Optimal Result

The results from the DIDO program for a a set of final configurations is provided in Fig 4-5. The mass and geometry properties used for these computations were taken from the actual prototype and are summarized in Table 4.1.

Since the DIDO program does not take the necessary conditions of optimality as an input, there is no guarantee that the results are a global minimum.

| Parameter | Value |
|---|---|
| $L_1$ | 95.25 (mm) |
| $m_A$ | 0.1 (kg) |
| $m_B$ | 0.12 (mm) |
| $m_C$ | 0.1 (kg) |
| $b_\phi$ | 41 (mNs/m) |
| $b_\theta$ | ~0 (mNs/m) |

Table 4.1: A list of the geometric and mass properties

The Karush-Kuhn-Tucker (KKT) conditions for optimality can be used to evaluate the optimality of our results [16]. Specifically, the condition for optimality is provided in eq. 4.21. In this equation, $\mu_X$ and $\mu_u$ represent the covector functions for the state variable, and control variable constraints. $\lambda$ represents the costates, and $u$ represents the input to the system (in this case $u = \tau$).

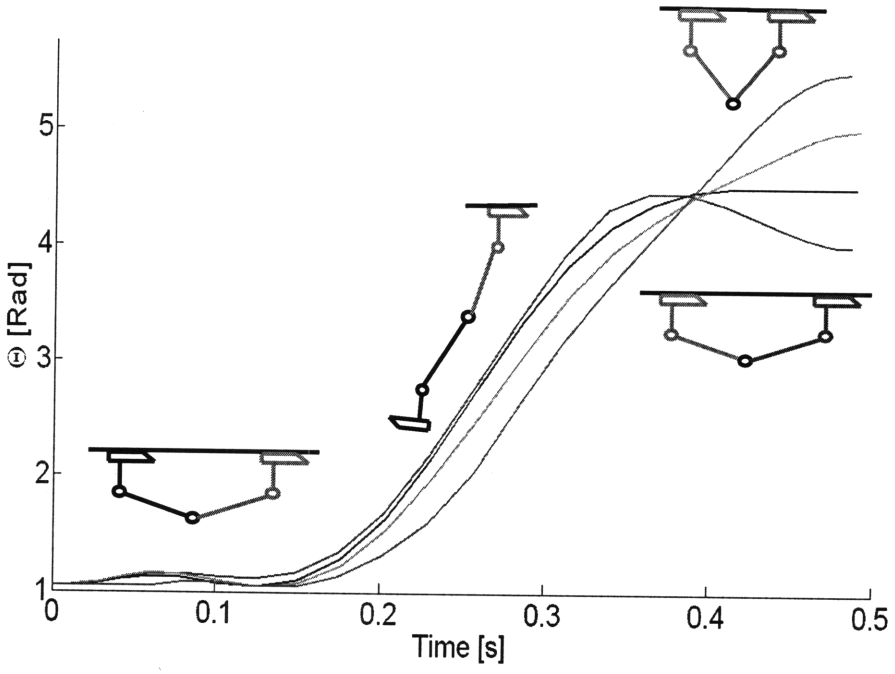


Figure 4-5: An illustration of the pseudo-optimal trajectories. The cartoon images illustrate the overall shape of the swinging motion as well as the different landing configurations

$$\frac{\partial \bar{H}(\mu_X, \mu_u, \lambda, X, u, t)}{\partial u} = 0 \tag{4.21}$$

$\bar{H}$ represents the Lagrangian of the Hamiltonian and is provided in eq. 4.24.

$$\dot{X} = F(X, u, t) \tag{4.22}$$

$$L(X, u, t) = (F_x^A)^{10} \tag{4.23}$$

$$\bar{H}(\mu_X, \mu_u, \lambda, X, u, t) = F(X, u, t) + \lambda^T L(X, u, t) + \mu_X^T X + \mu_u^T u \tag{4.24}$$

$$\frac{\partial \bar{H}}{\partial u} = \frac{\partial F}{\partial u} + \lambda^T \frac{\partial L}{\partial u} + \mu_u^T \tag{4.25}$$

We can evaluate eq. 4.25 using the results of the DIDO program. In general, solutions the solutions we obtained by the DIDO program did not suitably satisfy the

sufficient conditions for extremality. This is not completely unexpected due to the fact that the DIDO program does not explicitly solve the boundary value problem. While the results could probably be improved by using more mesh points and adjusting the nature of the equations, such steps add time and complexity. Therefore we will use the results in Fig. 4-5 and describe them as "Pseudo-Optimal" trajectories. We will use these results to provide insights into the basic shape and timescales of the desirable trajectories.

### 4.4.5 Search Program

In lieu of the fact that the numerical solution does not provide a global maximum it is good practice to attempt to verify our solution using an alternative method. Unfortunately, as we have discussed in detail, this type of Optimal Control problem is not easy to solve. Therefore to verify our pseudo-optimal solution we chose to use a search program to arbitrarily develop trajectories and then evaluate them based on our boundary conditions and the mini-max criterion. For the sake of physical intuition we used $\theta(t)$ as the pseudo input to our system (rather than the actuator torque $\tau$). The use of $\theta(t)$ as a pseudo-input is justified assuming a high fidelity feedback control for $\theta(t)$. Feedback linearization, for example guarantees convergence of $\theta(t)$ trajectories to a desired one $\theta_d(t)$ at an arbitrary convergence rate. Assuming such a high fidelity control for $\theta(t)$, we can treat $\theta(t)$ to be the input for controlling the underactuated system. The resulting dynamic equations for $\phi(t)$ are provided in eq. 4.26 and eq. 4.27. Note that now $\theta(t)$, $\dot{\theta}(t)$ and $\ddot{\theta}(t)$ are now inputs to the system.

$$\tau = H_{11}\ddot{\theta} + H_{12}\ddot{\phi} + C_{11}\dot{\theta} + C_{12}\dot{\phi} + G_1 \tag{4.26}$$

$$\ddot{\phi} = (H^{-1})_{21}\tau - (H^{-1}C)_{21}\dot{\theta} - (H^{-1}C)_{22}\dot{\phi} - (H^{-1}G)_2 \tag{4.27}$$

Trajectories were developed by connecting a set of 6 data points using a polynomial spline. The points can be divided into 3 groups. There were 2 "initial points" which were fixed to best accommodate the initial conditions. There were also 2 "final points" that were fixed to accommodate the final conditions. Finally, the 2 "inner points"

were modulated to create a variety of trajectory shapes. Both the value and the time value of each inner point were modulated. Therefore the search space was essentially 4 dimensional. A maximum time of $t = 0.6s$ was imposed on the trajectories in order to ensure that the search space was finite. This time was similar to the bound placed on the landing time $t_f$ used in the DIDO program. Trajectories that satisfied the boundary conditions were designated "acceptable trajectories." An illustration of some of the acceptable trajectories is provided in 4-6.

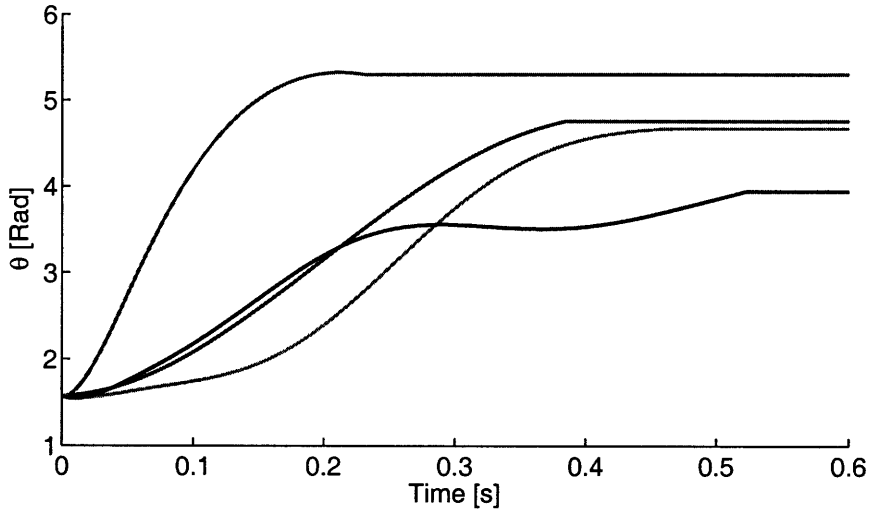


Figure 4-6: A plot illustrating some of the acceptable trajectories generated by the search program.

The trajectories that best minimized $max(F_x^A)$ were chosen. These are provided in 4-7. It is very important to note the limitations of this approach. There could be better trajectories that evolve over a longer time scale, trajectories with higher frequency components, and even trajectories that were missed due to the design of the search program. In addition, the result is dependent on the spacing of the mesh. However, the intention in this case was not to find the absolute best trajectory but instead to examine some optimal shapes and see how they compare to the pseudo-optimal results of the DIDO program. Despite these caveats there does exist a qualitative similarity between the results of the search program and the psuedo-optimal results (see Fig. 4-10). This similarity lends some legitimacy to the shape of our pseudo-optimal results.

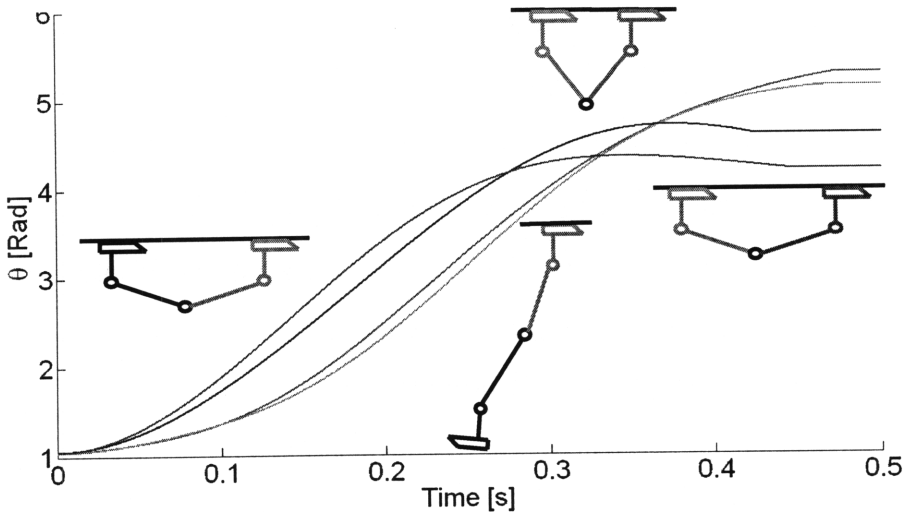


Figure 4-7: A plot illustrating the best trajectories generated by the search program.

## 4.5 Parametric Approach

Since the numerical solution to the optimal control problem is very time consuming, it is not a practical approach to generating trajectories. A more efficient methodology is desired. One possible solution is to parameterize trajectories using a smaller set of parameters. In this case, a cursory examination of the near optimal trajectories reveals that the trajectories all have a similar shape that resembles the combination of sigmoid functions. The trajectories for small landing angles ($\theta_f \sim 4.0$) have a small overshoot bulge while the the trajectories with larger landing angles are slower to evolve and resemble single sigmoid functions.

Therefore, an alternative to the optimal control formulation is to again treat the the actuated hip joint ($\theta$) as the "pseudo input" to the system and then attempt to generate parametric trajectories using a combination of sigmoid functions. To create the trajectory shape we will use the form provided in [18] and create the desired shape by smoothly joining 2 sigmoid functions. One major advantage of this formulation is that $\theta(t)$ is smooth and the derivatives ($\dot{\theta}(t)$ and $\ddot{\theta}(t)$) are continuous.

$$\theta(t) = \begin{cases} 0 \leq t \leq t_1 \\ \left[10\left(\frac{t}{t_1}\right)^3 - 15\left(\frac{t}{t_1}\right)^4 + 6\left(\frac{t}{t_1}\right)^5\right]\delta_1 + \theta_i \\ \\ t_1 \leq t \leq (t_1 + t_2) \\ t_2 = t_f - t_1 \\ \left[10\left(\frac{t-t_1}{t_2}\right)^3 - 15\left(\frac{t-t_1}{t_2}\right)^4 + 6\left(\frac{t-t_1}{t_2}\right)^5\right](\theta_f - \delta_1 - \theta_i) + (\theta_i + \delta_1) \end{cases} \tag{4.28}$$

Note that $\theta_i$ and $\theta_f$ represent the initial and final hip angle respectively. An illustration of the parameters $\delta_1, t_1, t_2$ is provided in Fig. 4-8. Also it is important to note that this formulation preserves the boundary conditions on $\theta(t)$ outlined in eq. 4.17 and eq. 4.18.

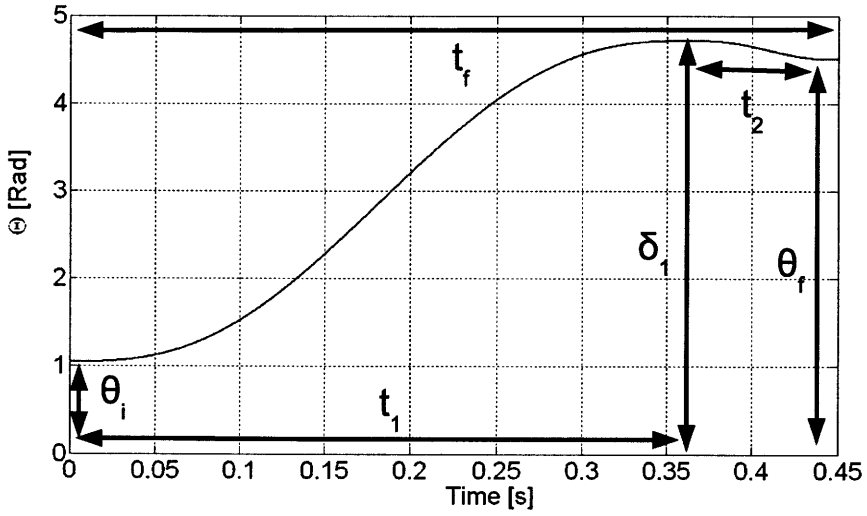


Figure 4-8: A plot illustrating the double sigmoid parameterization

Note that this leaves 3 parameters to be determined. We have a 2nd order boundary value with 4 boundary conditions. This means are system is indeterminate. However, if we choose to solve the problem as a set of boundary value problems where we specify the landing time $t_f$, we are left with only 2 parameters to determine. Using

the boundary conditions for $\phi(t)$ we were able to generate parameterized trajectories by solving the two point boundary value problem. Note that we had to solve for multiple landing times ($t_f$). This is due to the fact that for certain landing times a viable trajectory may not even exist. The pseudo-optimal results from the DIDO program illustrate that the landing times are all between 0.4s and 0.5s. This observation allowed us to reduce the search space for $t_f$ considerably.

The parametric trajectories that best minimized the reaction force $F_x^A$ were chosen as our "paramterized trajectories". An illustration of these results is provided in Fig. 4-9. Note the qualitative similarity between the parametric results and the pseudo optimal results (Fig. 4-10).

In addition a summary of the results is provided in Fig. 4-11. The results in this figure are particularly useful if a user does not have strict requirements on the landing conditions. The user can then select the $\theta_f$ that best reduces the reaction force. As the results illustrate, the trajectories with larger landing angles provide the lowest reaction forces. Therefore an easy rule of thumb would be to use the maximum allowable landing angle.

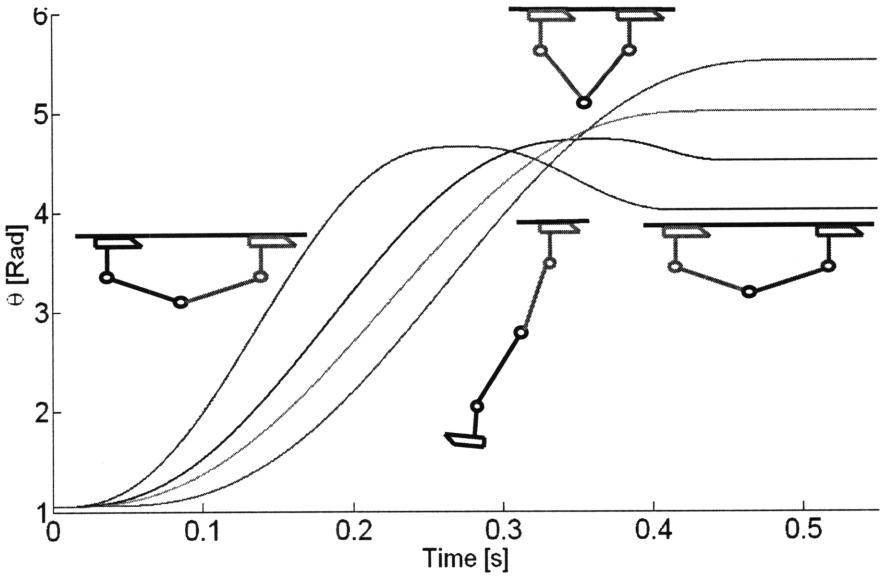


Figure 4-9: An illustration of the parametric trajectories. The cartoon images illustrate the overall shape of the swinging motion as well as the different landing configurations

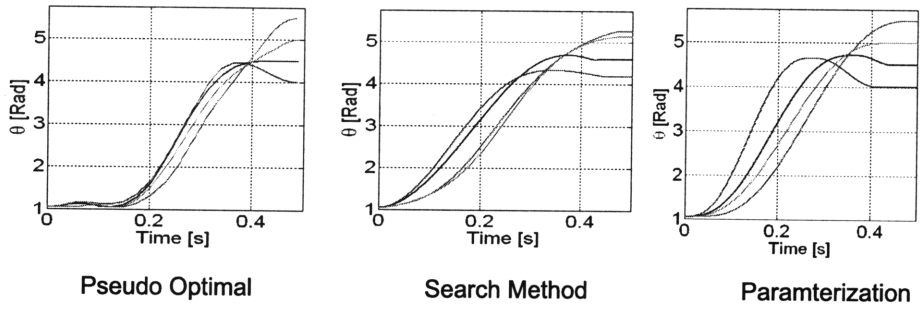


Figure 4-10: A side by side comparison of the psuedo optimal, search program, and parametric approach.

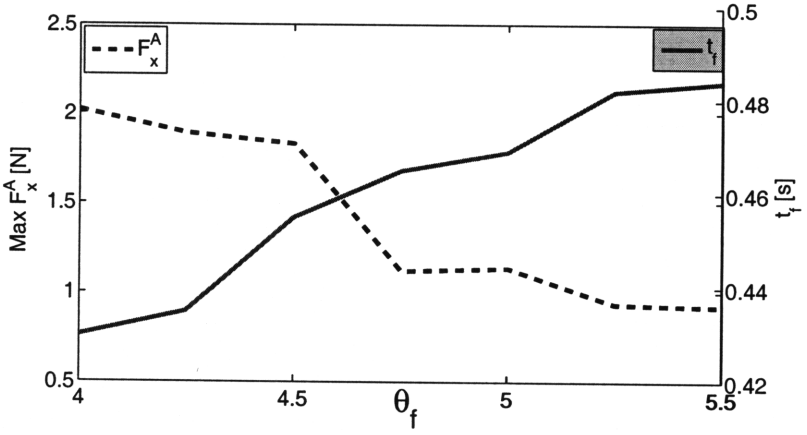


Figure 4-11: A plot illustrating the maximum reaction force (dashed line) and the landing time (solid line) for a number of landing configurations

# Chapter 5

# Implementation

In order to test and evaluate the concepts behind the Mag-Foot design, a small, fully functional prototype was designed and constructed. In addition, a test structure with a steel surface was constructed along with safety features to allow for controlled experiments.

## 5.1 Mechanism Design

While the discussions in this paper have focused on a planar design, a three-leg design was used to resist moments about the $y$ axis. The design consists of two leg pairs: an outer leg pair which consists of two legs coupled to a single shaft and an inner leg which is coupled directly to the motor housing. This design scheme allows the robot to perform all three gait modes. A solid model of the overall design is provided in Fig. 5-2.

## 5.2 Tilting Foot

In order to facilitate tilting, cylindrical magnets with a small radius were chosen for the feet. To this end the magnets were arrayed parallel to and as close as possible to the tilting edge of the foot. Care was taken to place the magnets far enough apart to reduce interference. 6mm diameter, nickel plated N38 magnets (attachment force

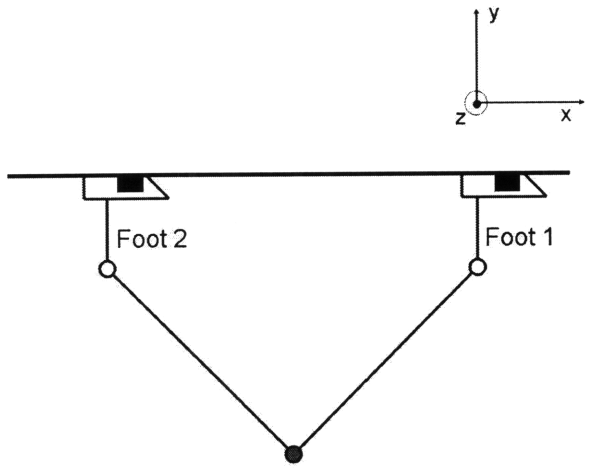


Figure 5-1: A diagram illustrating the basic mechanism structure and the coordinate frame.

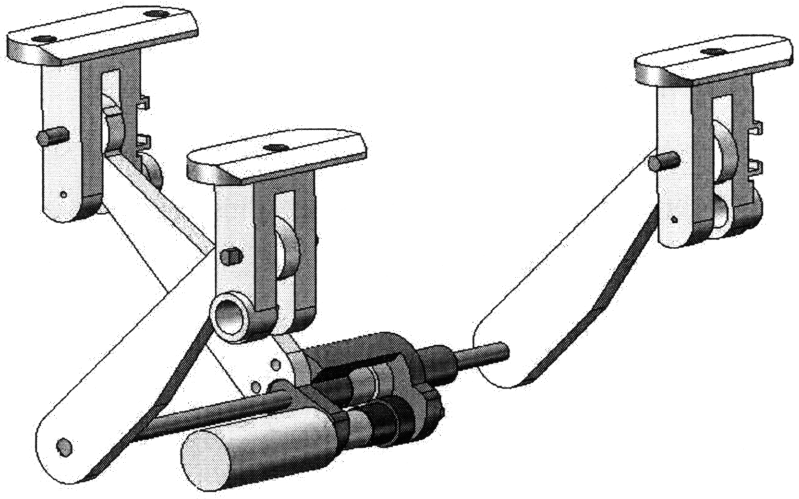

Figure 5-2: A solid model illustrating the 3 dimensional nature of the final design.

4N) were used for the feet. An illustration of the tilting foot design is provided in Fig. 5-3.

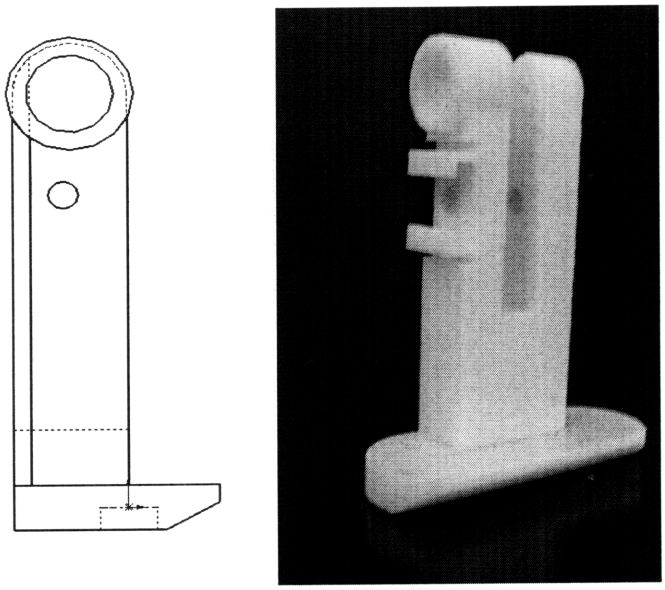

Figure 5-3: An illustration of the tilting foot design.

## 5.3 Ankle Locking Mechanism

Once Foot 2 is tilted (Foot 1 remains planted, see Fig. 5-1) it must be detached from the surface by pushing the legs apart using the DC motor at the hip. However, these forces also act to make the foot tilt back into its planted configuration. Therefore a locking mechanism must be used to keep Foot 2 in its tilted configuration. A design for a locking mechanism for the ankle was created using a solenoid. The solenoid rod acts as a sort of deadbolt to lock the foot in relation to the leg. The geometry of the leg allows the solenoid to engage only once the foot is tilted and prevents any subsequent rotation. This mechanism was designed so that rotation in one direction is allowed but is blocked in the other direction. This allows the foot to rotate freely in order to align itself with the surface when it lands. Note that the ankle joint in the planted foot (Foot 1) remains unlocked in order to allow free rotation for the swinging motions. It should also be noted that due to the use of the deadbolt type configuration, the force requirements for the solenoid are very low (the load is

applied orthogonal to the direction of motion and is therefore taken up by the bearing and rod). In addition, since no feedback is required, these locking mechanisms are extremely simple and fairly lightweight. An illustration of the locking mechanism is provided in Fig. 5-4.

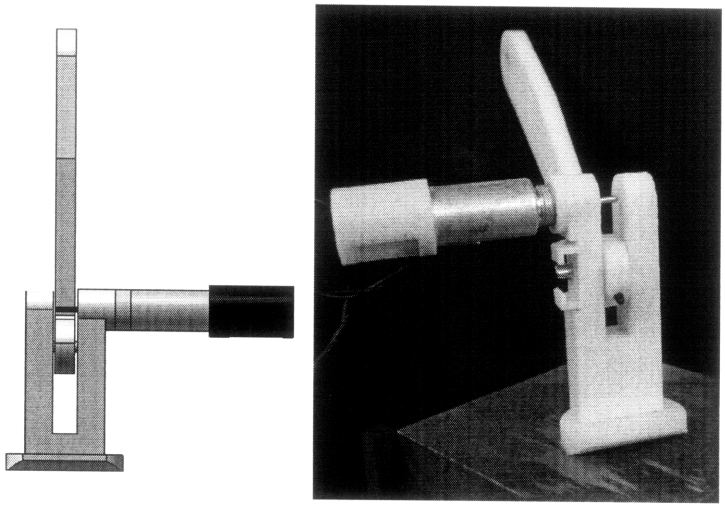

Figure 5-4: An illustration of the locking mechanism design.

## 5.4 Fabrication and Actuation

The components with complex geometry such as the motor housing and the tilting feet were constructed from ABS plastic using a FDM style 3D printing machine (Dimension SST 2300). The hip joint was actuated by a NiDec Copal 12V DC Planetary Gearmotor (60:1 reduction, Part No. HG-16-120-AB).

## 5.5 Sensing and Control

A 10 bit absolute magnetic shaft encoder (US Digital) was used to measure the hip angle. An angle-sense potentiometer can be coupled to the ankle shaft to measure the angle between the leg and the foot. A National Instruments CompactRIO System (CRio 9074) was used for data acquisition and control. The CRIO system uses an

FPGA for lower level tasks such as hardware interfacing and closed loop control. This enables the use of sampling frequencies in the MHz range. For our case the sampling rate is limited by the sensors to 2KHz. However, this is more than sufficient for the swinging motions which evolve over $\sim$ 0.5s. Custom written Labview software was used for the CRIO system. It should be noted that the initial Mag-Feet prototype is a tethered system; it is connected via thin cables to a DC power supply as well as to the CRIO system.

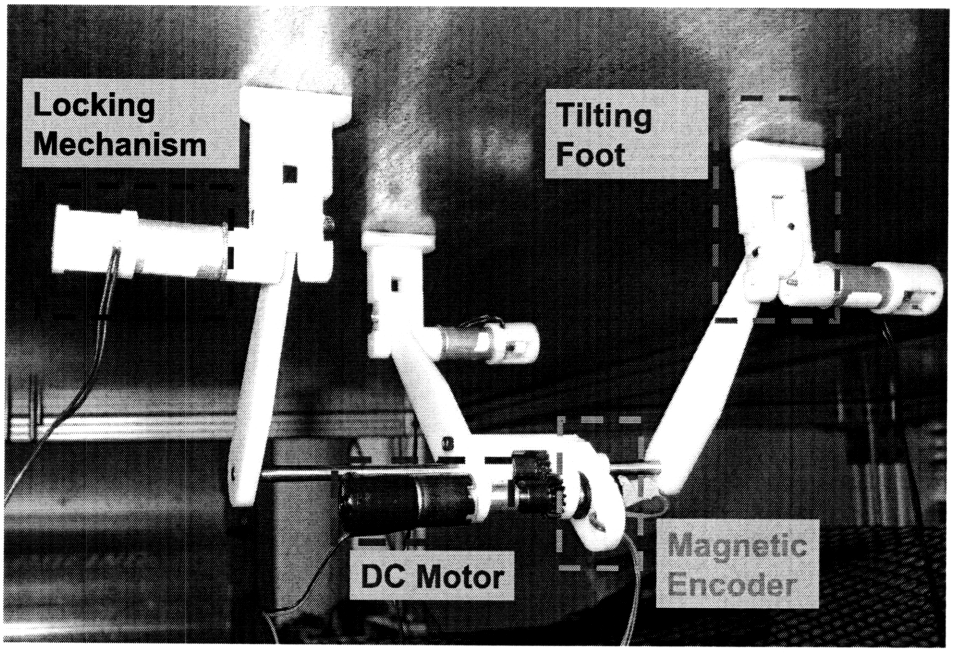


Figure 5-5: A photograph of the entire Mag-Feet Robot prototype.

## 5.6 Changing Plane of Motion

It should be noted that with this design and implementation, the motion is restricted to the $xy$ plane. In addition, the device can only move in one direction. Fig. 5-6 illustrates our proposed solution. A DC Motor (labeled in red) would be placed in the tilting foot of the inner leg allowing rotation about the $y$ axis. Note that now the inner foot has radial symmetry. A "heel" is used to prevent the inner foot from tilting backwards. The "heel" rotates with the ankle assembly (labeled in green).

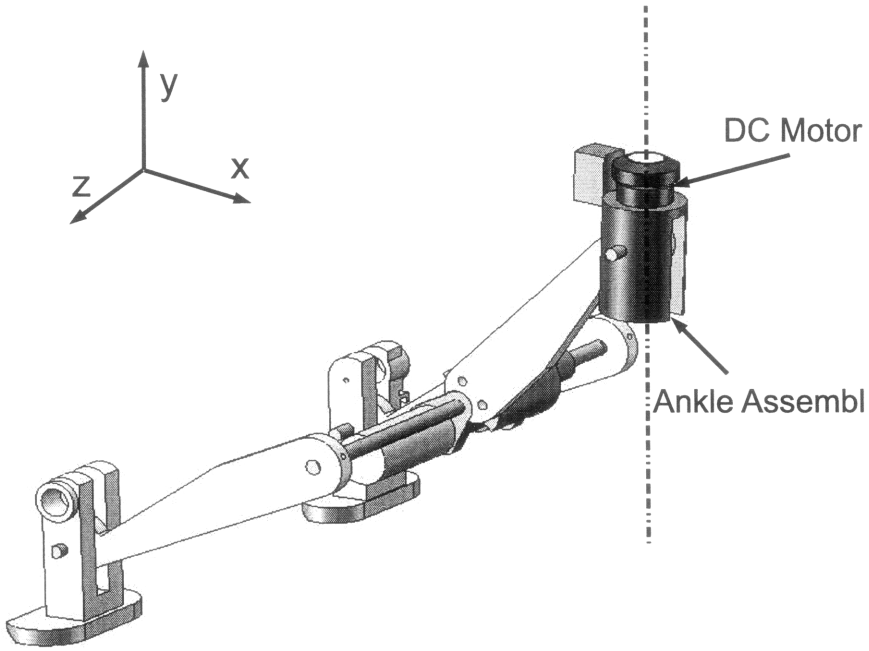


Figure 5-6: A solid model of the design concept for changing the plane of motion.

The change of direction sequence would be as follows. First, the outer feet are tilted and detached. Once the robot is hanging only by its inner foot, the DC motor in the inner foot is used to rotate the device to the proper plane of motion. Finally, parametric excitation can be used to swing the outer feet back up to the surface. Some methods for solving the "swing up" problem are provided in [9]and [10].

This addition to the design is essentially independent of the design we have already outlined. Therefore it was omitted from the implementation so that we could focus on the more fundamental features of the device such as the tilting foot and the swinging problem. It is hoped that future designs will include this feature.

## 5.7 Instrumented Foot

For the swinging experiments it was desired to measure the forces applied to the planted foot in addition to the ankle angle. Therefore a special instrumented foot was constructed. This foot was not designed for motion but instead to simply measure the

forces and angles at the planted foot. The foot was equipped with a potentiometer to measure the ankle angle and a load cell (Transducer Techniques MLP-10) for measuring the reaction force in the $x$ direction.

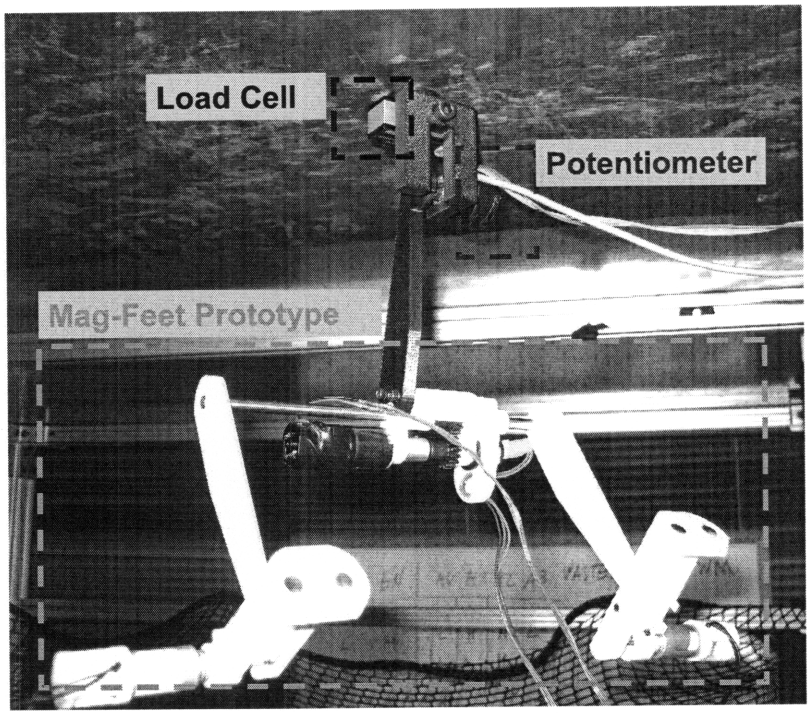


Figure 5-7: A photograph of the instrumented foot used for the swinging experiments.

# Chapter 6

# Results

The Mag-Feet prototype was evaluated at the D'Arbeloff Laboratory at MIT. A series of experiments were performed with the goal of determining the feasibility and effectiveness of the methods and designs outline in this thesis. To this end several studies were performed. The Moonwalk and Shuffle gaits were evaluated using a simple controller. Finally, a set of more comprehensive experiments were performed to evaluate our proposed parameterized solution to the swinging problem.

## 6.1 Sliding Primitive

The sliding primitive is used for both the Moonwalk and the Shuffle gait modes. As discussed in Chapter 3, the sliding primitive can be described using a 4 bar linkage. The kinematics are described completely by the hip angle $\theta$. Therefore the sliding mode gait becomes a closed loop servo control problem. A Proportional + Integral (PI) controller was used to control the hip angle for gait control.

### 6.1.1 Moonwalk Results

An illustration of the Moonwalk results is provided in Fig. 6-1. This figure provides several insights. First, the Moonwalk gait is indeed feasible and can be achieved using a classical controller. In addition, these results illustrate the the device can

indeed pass successfully through the singular configuration provided that the surface is relatively horizontal. Finally, it is worth noting that while the robot moves fairly slowly ( it takes 2 steps in 8 seconds), the goal of the experiment was not to determine performance limits but rather to determine feasibility. If increased walking speed is desired, the controller gains can be appropriately adjusted.

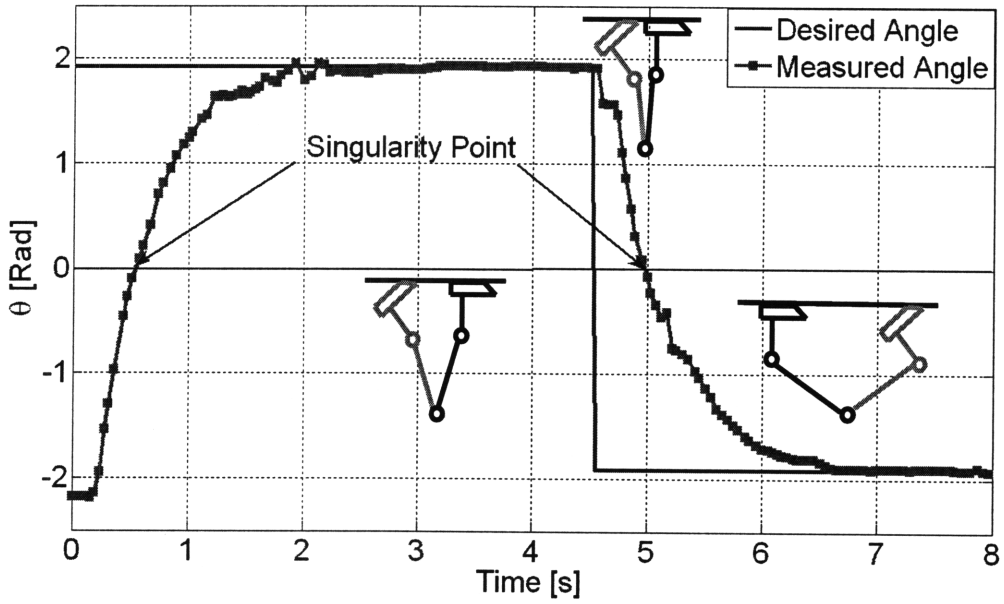


Figure 6-1: A plot illustrating the closed loop control of the hip angle ($\theta$) during the Moonwalk gait. Note how the mechanism passes through the singular configuration. The cartoon illustrates the actual configuration of the mechanism at certain points in the gait cycle.

### 6.1.2 Shuffle Results

An illustration of the Shuffle results is provided in Fig. 6-2. This figure reveals that the Shuffle gait is also feasible and like the Moonwalk gait can be achieved using a classical controller. Note how in this case the mechanism avoids the singular configuration ($\theta = 0$). Note that this experiment was also performed on a horizontal steel surface. Very simple experiments have revealed that the Shuffle gait can also be used on surfaces with slight inclines and declines. Clearly there will exist maximum and minimum angles that will limit the device. These limits can be determined

analytically using the models outlined in Chapter 3.

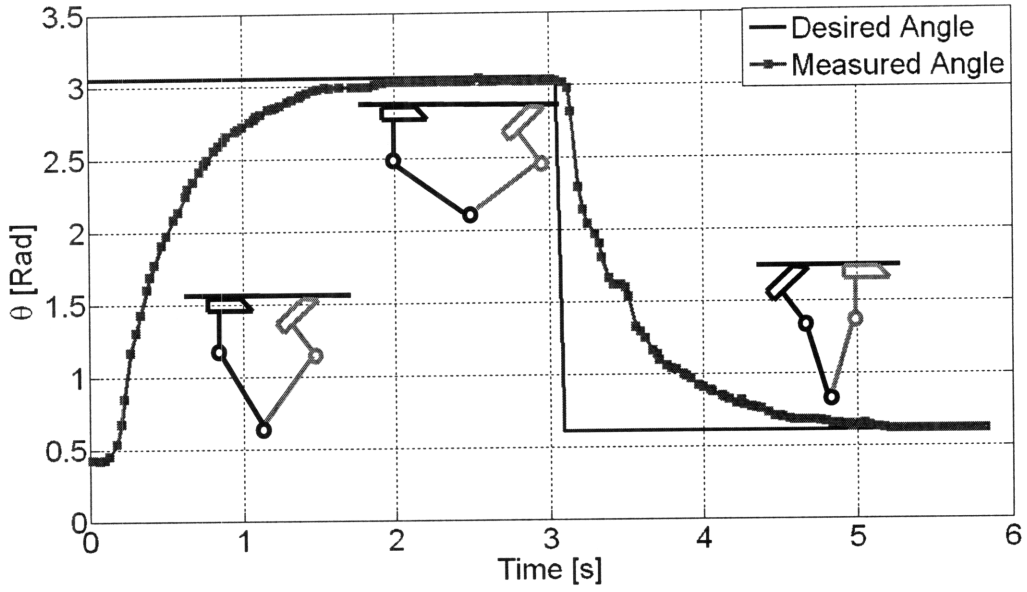


Figure 6-2: A plot illustrating the closed loop control over the hip angle ($\theta$) during the shuffle gait. The cartoon illustrates the actual configuration of the mechanism at certain points in the gait cycle.

## 6.2 Swinging Experiments

### 6.2.1 Introduction

A detailed study was performed to evaluate the proposed method for parameterizing minimum reaction force trajectories using sigmoid functions. These experiments were motivated by the observation that many trajectories can violate the reaction force constraints and cause the planted foot to first tilt and then detach, causing the robot to fall. Video evidence of this phenomenon is provided in Fig. 6-3.

### 6.2.2 Experimental Setup

Since the focus of the swing experiments was to characterize the swinging motions, a tethered setup was used. Thin wires were used to connect the robotic device to

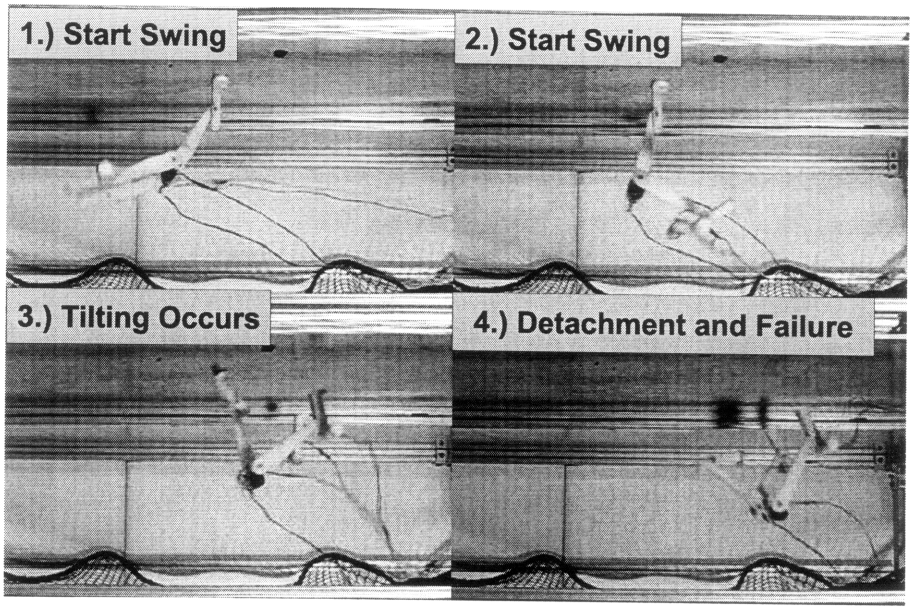


Figure 6-3: A set of video frames illustrating the failure mode when the reaction force constraints are exceeded.

the power supply and control system. Care was take to minimize the effects of these wires on the swinging dynamics. The experiments were carried out on an elevated horizontal steel surface. The experimental procedure consisted of manually placing the robot in the configuration described by the initial conditions with the ankle locking mechanisms engaged. While it is desired that the robot first servo the legs and then lock them, the manual approach was used to improve repeatability and to avoid unnecessary stress on the components. Once the locking mechanism was engaged the "swing command" was given to the system. Due to the use of the instrumented foot, only half the swing gait was performed. The swing gait was performed using the outer feet due to the fact that landing is more difficult due to the fact that both feet must land properly. If two feet can land properly there is no reason that the inner foot cannot do so as well. We chose one parameterized trajectory for detailed study and analysis. The landing angle of $\theta_f = 4.5$ was chosen because it as considered to be a representative landing configuration (not too wide or too narrow). In addition, this trajectory is a good choice for detailed study because the parameterized trajectory is

relatively complex (it contains an overshoot bulge, see Chapter 4). The experiments were carried out using the National Instruments CRio system described in Chapter 5. Closed loop control was performed on the FPGA system at a sampling rate of 2 KHz. The trajectory generation was performed on the real time computer and operated at 500 Hz. Linear interpolation was used to fill in the points.

### 6.2.3 Initial Compensator

For the sake of simplicity and ease of implementation we began with a classical controller. Specifically, we used a Proportional plus Derivative (PD) controller. To improve speed of response feedforward velocity and acceleration terms were used. The use of a polynomial to create the sigmoid functions greatly simplified the implementation of feedforward control since the derivatives could be determined analytically. A block diagram is provided in Fig. 6-4. The gains were tuned manually to achieve the best performance.

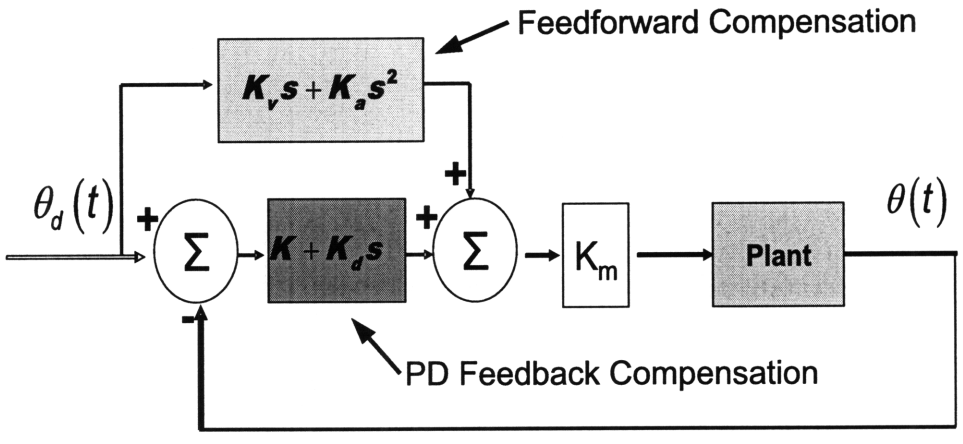


Figure 6-4: A diagram illustrating the initial PD Compensator with additional feedforward terms.

### 6.2.4 Initial Experimental Results

The results of the initial experiments are provided in Figs. 6-5 to 6-7. It should be noted that the results are highly dependent on the initial conditions and are therefore not entirely consistent. As a result there were experiments where the device either landed too hard or failed to land at all. The results provided are intended to be a typical result.

The trajectory of the actuated joint $\theta(t)$ is provided in Fig. 6-5. The figure illustrates that the controller does a satisfactory job of tracking the overall shape of the parameterized trajectory. Note that the overshoot bulge is replicated. There does exist a small delay of 20ms but the delay in itself is not harmful as long as the trajectory shape is reproduced.

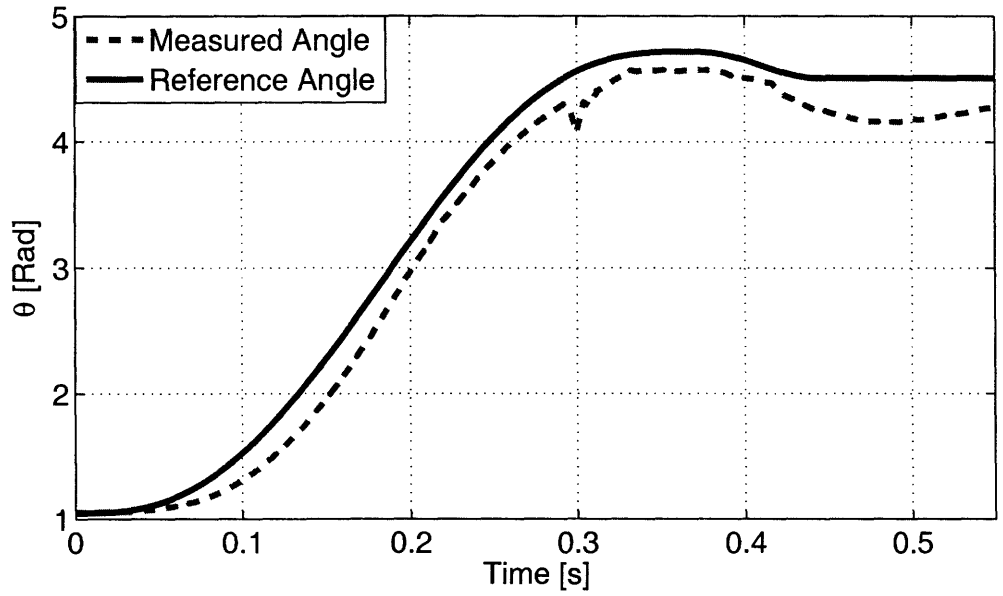


Figure 6-5: A plot comparing the parameterized pseudo input with the measured hip angle ($\theta$).

The trajectory of the unactuated joint $\phi(t)$ is provided in Fig. 6-6. This plot illustrates that while the shapes are similar, there do exist visible deviations from the trajectory predicted by the model. These deviations are especially evident during the beginning of the trajectory ($t = 0s$ to $t = 0.2s$).

Finally, the x direction reaction force profile $F_x^A(t)$ is provided in Fig. 6-7. This

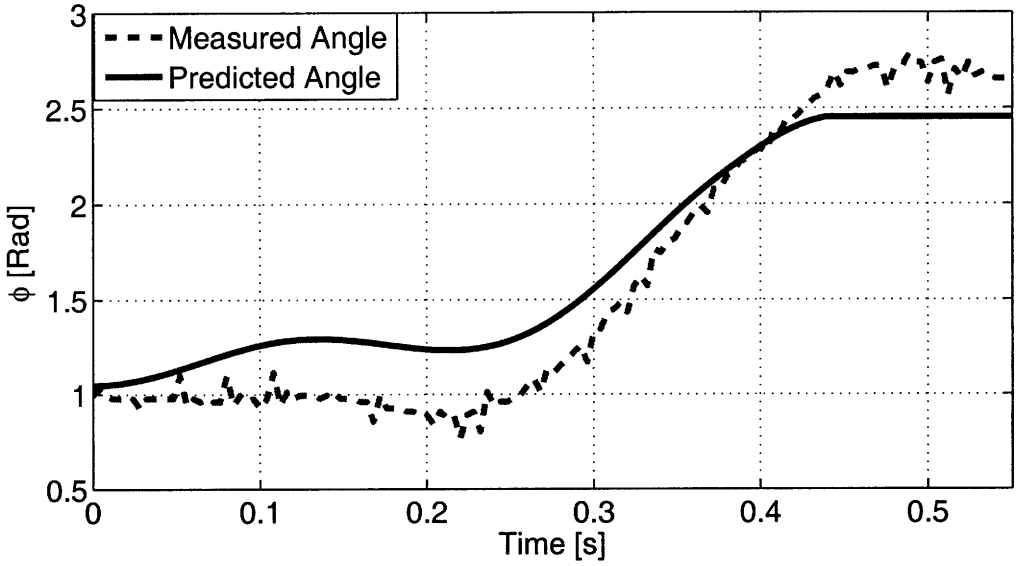


Figure 6-6: A plot comparing the predicted unactuated trajectory ($\phi$) with the measured result.

plot illustrates qualitative between the measured force and the forces predicted by the model. Of particular significance is the maximum force peak. Note how the maximum measured reaction force is within 10 percent of the model prediction. Despite this error the measured reaction force remains $\sim$ 0.5N below the threshold of 2.5N. While this margin is small in absolute terms, it is about 25 percent.

A plot of the measured reaction force profile for a "bad" sigmoid trajectory is provided in Fig. 6-8. Note how this trajectory violates our reaction force constraint. Also of interest is the hard landing. This is visible from the large spike in force at $t \sim 0.4s$ and the resulting fluctuations due to vibrations in the test structure. This illustrates how trajectories that are not properly selected can potentially lead to failure.

### 6.2.5 Discussion

These initial results are promising. They illustrate that under certain conditions, the dynamics seem to match the prediction well. Most importantly, the maximum reaction forces is very close to the prediction. This means that our trajectories should not cause the planted foot to tilt or detach. Nevertheless there exist discrepancies

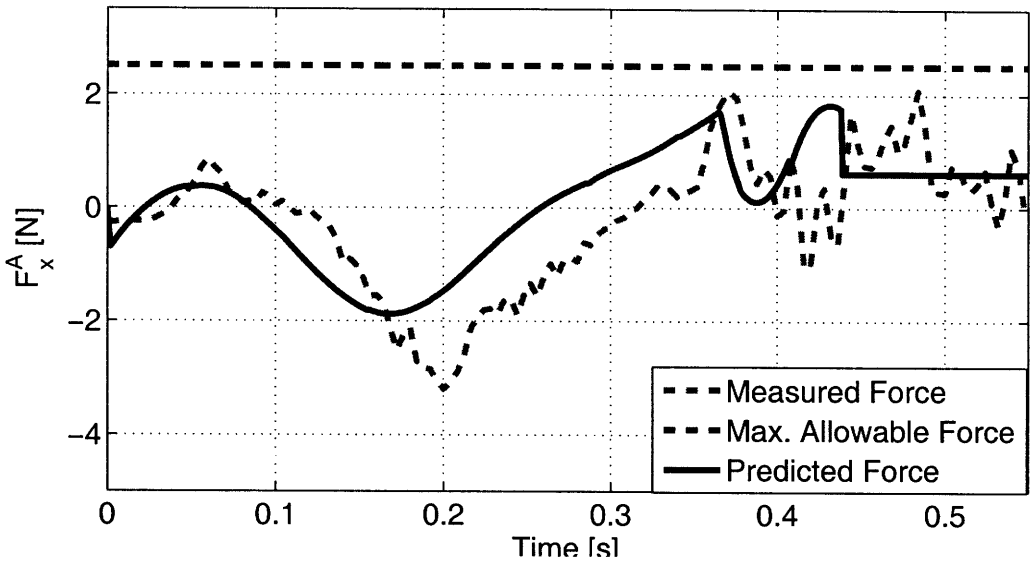


Figure 6-7: A plot comparing the predicted reaction force $F_x^A$ with the measured result.

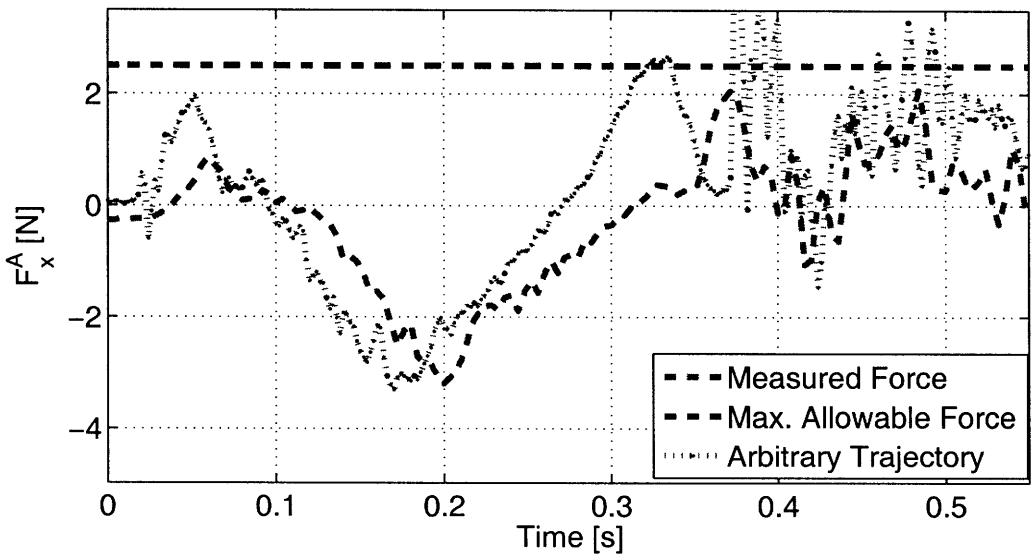


Figure 6-8: A plot comparing measured data from two trajectories. The optimized parametric trajectory is labeled in red while the "bad" trajectory is labeled in green. Note how the "bad" trajectory violates the force constraint.

between the model predictions and the measured results. Possible sources include the interference caused by the wires and nonlinear effects in the DC motor. In addition, the initial conditions are a source of error. The DC motor must pull the locked foot off the surface in order to initially detach it. This means that when the foot release there is a recoil effect where the foot will accelerate away from the surface once it detaches. This is due to the fact that the magnetic attraction force decreases with distance. An important concern is properly tracking the parameterized trajectory. If the pseudo input does not track the desired trajectory, it is certainly expected that the overall system will deviate from the model predictions. This was observed experimentally as there were trajectories that did suffer from pronounced tracking problems. These problems persisted despite tuning of the feedback and feedforward gains. This result isn't altogether surprising, as convergence as only guaranteed using feedback linearization rather than PD control. In this regard, this trajectory illustrates the limitations of a simple PD controller. In addition, there is the presence of the "notch" in the measured $\theta(t)$ trajectory which occurs at $t \sim 0.3s$ (see Fig. 6-5). This notch is likely the result of backlash in the mechanism (the motor is forced to change direction ). While this does not appear to be a major problem with this trajectory it certainly has the potential to complicate matters. This problem could be solved by replacing the spur gear transmission with a belt drive. Future revisions to the design will include this change.

### 6.2.6 Revised Compensator

The difficulties in tracking the parameterized trajectory stem from the fact that the system is nonlinear and subject to a number of disturbing torques. The dynamics for $\theta(t)$ are provided in eq. 6.1.

$$H_{11}\ddot{\theta} = \tau - H_{12}\ddot{\phi} - C_{11}\dot{\theta} - C_{12}\dot{\phi} - G_1 \tag{6.1}$$

However, since the model structure and model parameters are well known we can use some nonlinear controls tools. Specifically we can employ feedback linearization

(also called Computed Torque Control). This involves using knowledge of the model and feedback from the system to cancel out all the nonlinear dynamics. Using this approach we can compute the torque $\tau$ to apply to the system. Note, we assume that $\lambda$ is a positive constant. For definitions of $G, H, C, \tau$ see Chapter 4.

$$\tilde{\theta}(t) = \theta_d(t) - \theta(t) \tag{6.2}$$

$$\tau = H_{11}(\ddot{\theta}_d + 2\lambda\dot{\tilde{\theta}} + \lambda^2\tilde{\theta}) + C_{11}\dot{\theta} + C_{12}\dot{\phi} + G_1 + H_{12}\ddot{\phi} \tag{6.3}$$

Plugging in this result for $\tau$ causes the the system dynamics to simplify considerably.

$$\ddot{\tilde{\theta}} + 2\lambda\dot{\tilde{\theta}} + \lambda^2\tilde{\theta} = 0 \tag{6.4}$$

With this compensator design, it is clear that $\theta(t)$ eventually converges to $\theta_d(t)$. This compensator design could be used in the future to improve the tracking of the parametric trajectory.

# Chapter 7

# Conclusion

This work has described the design, analysis, and control of a new type of robot for the inspection of steel surfaces such as bridge members. We outlined a novel tilting foot design that allows us to modulate the force of permanent magnetic feet by introducing an air gap. We used this tilting foot to create a robotic device (titled "Mag-Feet") capable of three unique modes of locomotion; the moonwalk can be used for moving quickly along flat surfaces, the shuffle can be used for walking along surfaces with small inclines, and the swing can be used to traverse small obstacles. The "Mag-Feet" performs these actions while using only a single actuator in tandem with simple locking mechanisms.

In addition, we formulated the "swinging problem" in the context of minimizing the reaction forces at the planted foot during the swinging motion. This swinging problem is a result of the tilting foot design and is a unique constraint that to the best of our knowledge has yet to be addressed for these types of underactuated swinging motions. We developed "pseudo-optimal" trajectories by formulating the swinging problem as a minimax optimal control problem and then solving it numerically. The pseudo-optimal trajectories were then used to develop insights into the shape and timescale of trajectories. These insights were used to parameterize the input using sigmoid functions. The swinging problem was then solved as a non-linear two point boundary value problem.

Finally, we designed and constructed an initial prototype. Experimental studies

were used to verify the validity of the design as well as the efficacy of the moonwalk and shuffle gait modes. In addition, experiments were performed to evaluate our proposed parametric solution to the swinging problem. Preliminary results using a classical compensator were promising and revealed good correspondence with the predictions of the dynamic model.

There do exist limitations to the current design and implementation. First, the initial prototype is limited to a single plane of motion and is not capable of turning around. We have proposed a new design to address this, but this design must be verified physically. In addition, the magnetic feet are dependent on friction to tilt before sliding. Therefore the tilting feet are unsuitable for highly slippery surfaces. Also, this design is limited to walking upside down on relatively flat surfaces. While this may be sufficient to bridge surfaces, this is limits the applicability of the design. Finally, since the swinging motions are based on pre-computed trajectories they are dependent on initial conditions and outside forces. As a result, while promising results were obtained, there existed substantial variations in the results.

Future work includes the development of a large scale, untethered prototype. Such a device would likely eliminate some of the complications from wires and outside forces but constructing such a device will likely be a substantial undertaking. In addition, the inclusion of sensing methodologies would be valuable. One area that holds promise the use of magnetic flux leakage to detect cracks and corrosion. The permanent magnets in the feet could perhaps be used in tandem with hall effect sensors as a detection methodology. Finally, the swinging problem merits further exploration. We have only explored fairly basic compensator designs, drawing more from the nonlinear controls community would perhaps lead to better trajectory tracking results.

# Appendix A

# Tilting and Sliding Mode Statics for Inclined Surfaces

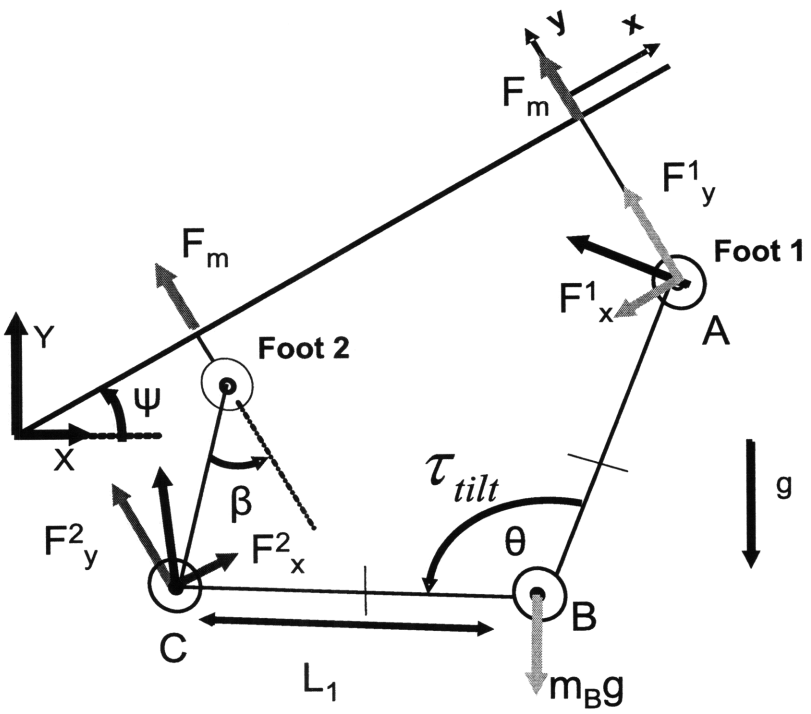


Figure A-1: A free body diagram for the inclined case.

First determine the reaction forces at the feet $R_1$ and $R_2$.

$$\varphi_1 = \frac{\pi}{2} - \frac{\theta}{2} \tag{A.1}$$

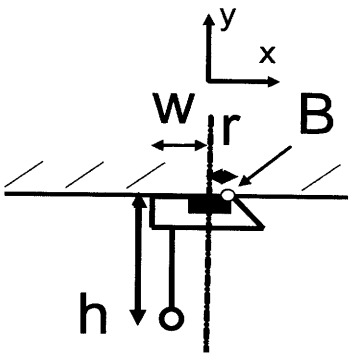


Figure A-2: An illustration of the tilting foot geometry.

$$\varphi_2 = \frac{\pi}{2} + \frac{\theta}{2} \tag{A.2}$$

$$R_1 \sin\varphi_1 + R_2 sin\varphi_2 = m_B g cos\psi \tag{A.3}$$

$$R_1 \cos\varphi_1 + R_2 \cos\varphi_2 = m_B g \sin\psi \tag{A.4}$$

$$R_1 = \frac{m_B g}{\sin\theta} \cos(\psi + \varphi_2) \tag{A.5}$$

$$R_2 = \frac{m_B g}{\sin\theta} \cos(\psi + \varphi_1) \tag{A.6}$$

Use geometry to determine the forces $F^1$ and $F^2$ applied to the feet by the DC Motor.

For the case where $\theta > 0$:

$$F_x^2 = -\frac{\tau}{L_1} \cos\frac{\theta}{2} \tag{A.7}$$

$$F_y^2 = -\frac{\tau}{L_1} \sin\frac{\theta}{2} \tag{A.8}$$

Now we can use a force balance at Foot 2 (the foot to be tilted or slid) to solve

for the torque $\tau$. Recall that $F_m$ represents the magnetic attraction force between the foot and the surface (acting in the $y$ direction).

$$\tau = \frac{(F_m r + R_2 h \cos\varphi_2 + R_2(w+r)\sin\varphi_2)\, L_1}{-h\cos\frac{\theta}{2} + (w+r)\sin\frac{\theta}{2}} \tag{A.9}$$

Once $\tau$ is determined the forces on the planted foot $(F_x^1, F_y^1)$ can be computed. This allows us to determine if failure will occur.

$$F_x^1 = \frac{\tau}{L_1}\cos\frac{\theta}{2} \tag{A.10}$$

$$F_y^1 = -\frac{\tau}{L_1}\sin\frac{\theta}{2} \tag{A.11}$$

We can perform the same analysis for $\theta < 0$. Note how the configuration of the system changes. Foot 2 (the one we are trying to manipulate by tilting or sliding) is now in front of Foot 1. Relations $A.1$ to $A.8$ still hold for this new configuration.

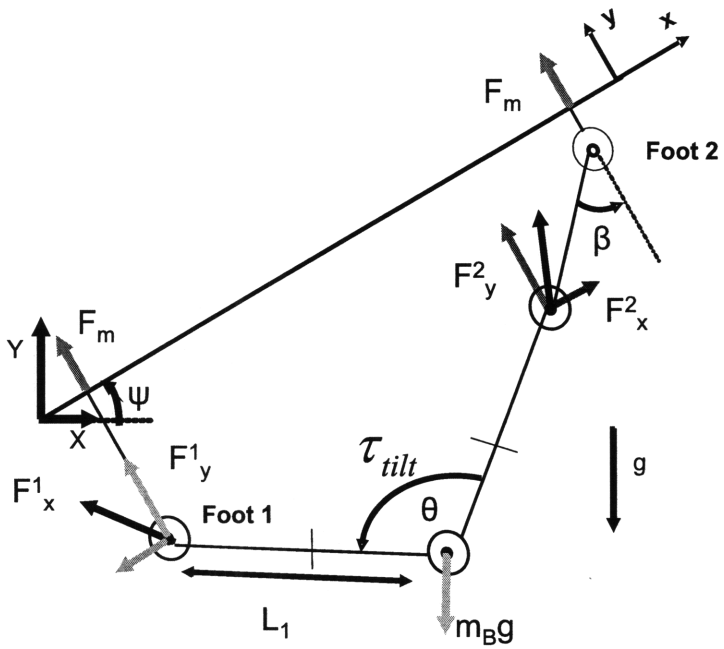


Figure A-3: A free body diagram for the inclined case, note how Foot 2 is now ahead of Foot 1.

Again we use geometry to determine the forces $F^1$ and $F^2$ applied by the DC Motor to the feet.

$$F_x^2 = \frac{\tau}{L_1} \cos\frac{\theta}{2} \tag{A.12}$$

$$F_y^2 = \frac{\tau}{L_1} \sin\frac{\theta}{2} \tag{A.13}$$

$$\tau = \frac{(F_m r + R_2 h \cos\varphi_2 + R_2(w+r)\sin\varphi_2)\, L_1}{h\cos\frac{\theta}{2} - (w+r)\sin\frac{\theta}{2}} \tag{A.14}$$

Once again, if $\tau$ is known it can be used to compute the forces on the planted foot (Foot 1).

$$F_x^1 = -\frac{\tau}{L_1} \cos\frac{\theta}{2} \tag{A.15}$$

$$F_y^1 = \frac{\tau}{L_1} \sin\frac{\theta}{2} \tag{A.16}$$

# Appendix B

# Magnet Information

GaussBoys (GaussBoys.com) Nd N38 Magnet. Diameter: 6mm; Thickness: 2mm; Pull Force: 8.9 N; Mass = 0.425g;

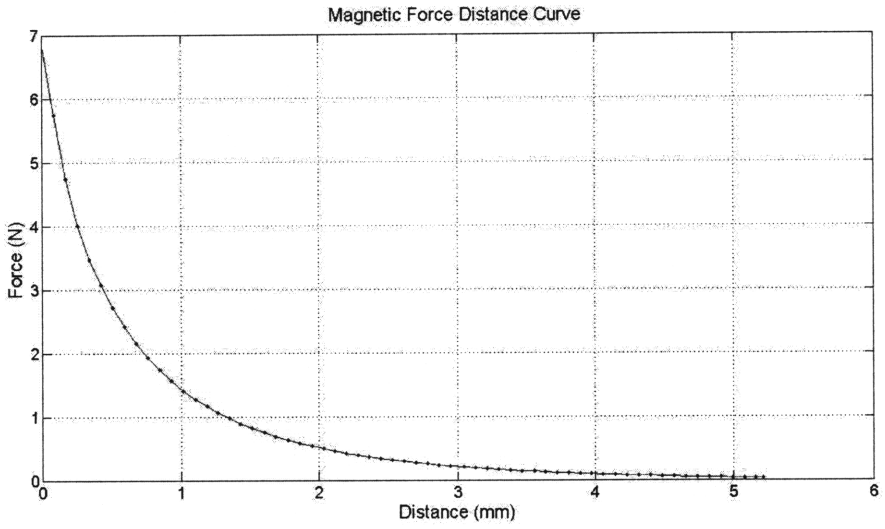


Figure B-1: A measured Force-Distance profile for the Magnet

# Bibliography


[1] "National bridge inventory data," tech. rep., U.S. Department of Transportation Federal Highway Administration, 2007.

[2] S. Watkins, "Smart bridges with fiber optic sensors," *IEEE Measurement and Instrumentation Magazine*, vol. 1094, 2003.

[3] "Reliability of visual inspection for highway bridges, volume i: Final report," tech. rep., U.S. Department of Transportation Federal Highway Administration, 2001.

[4] J.-K. Oh, A.-Y. Lee, S.-M. Oh, Y. Choi, B.-J. Yi, and H. Yang, "Design and control of bridge inspection robot system," in *Proceedings of the IEEE International Conference on Mechatronics and Automation*, pp. 3634–3639, August 2007.

[5] C. Balaguer, A. Gimenez, and M. Abderrahim, "Climbing robots for inspection of steel based infrastructures," *Industrial Robot*, vol. 29, no. 3, 2002.

[6] A. Slocum, S. Awtar, and A. Hart, "Magnebots: A magnetic wheels based overhead transportation concept," in *Proceedings of the 2nd IFAC Mechatronics Conference*, p. 833, November 2002.

[7] M. Menon and H. Asada, "Design of a semi-passive heavy duty mobile robotic system for automated assembly inside an aircraft body," in *Proceedings of the IEEE/RSJ International Conference on Intelligent Robots and Systems*, pp. 2429–2434, September 2008.

[8] C. Gosselin and J. Angeles, "Singularity analysis of closed kinematic chains," *IEEE Transactions on Robotics and Automation*, vol. 6, no. 3, pp. 281–290, 1990.

[9] J. Saito, T. Fukuda, and F. Arai, "Heuristic generation of driving input and control of brachiation robot," *The JSME International Journal*, vol. 37, no. 1, pp. 147–154, 1994.

[10] Y. Hasegawa, T. Fukuda, and K. Shimojima, "Self-scaling reinforcement learning for fuzzy logic controller - applications to motion control of two-link brachiation robot," *IEEE Transactions on Industrial Electronica*, vol. 46, no. 6, pp. 1123–1131, 1999.

[11] J. Nakanishi, T. Fukuda, and D. Koditscheck, "Brachiation on a ladder with irregular intervals," *Advanced Robotics*, vol. 16, no. 2, pp. 147–160, 2002.

[12] S. Dubowsky and E. E. Vance, "Planning mobile manipulator motions considering vheicle dynamic stability constraints," in *Proceedings of the IEEE 1989 International Conference on Robotics and Automation*, pp. 1271–1276, May 1989.

[13] H. Osumi and M. Saitoh, "Control of a redundant manipulator mounted on a base plate suspended by six wires," in *Proceedings of the IEEE/ RSJ International Conference on Intelligent Robots and Systems*, pp. 73–78, October 2006.

[14] C. Chung, S. Desa, and C. deSilva, "Base reaction optimization of redundant manipulators for space applications," tech. rep., The Robotics Institute Carnegie Mellon University, 1988.

[15] A. Bryson, *Applied Optimal Control: Optimization, Estimation, and Control.* New York: Hemispher Pub. Corp, 1975.

[16] I. Ross, "A beginner's guide to dido," tech. rep., Elissar, LLC, 1998.

[17] G. Michael, "Computation of chebycheff optimal control," *AIAA Journal*, vol. 9, no. 5, pp. 973–975, 1971.

[18] B. Roy and H. H. Asada, "Dynamics and control of a gravity-assisted underactuated robot arm for assembly operations inside an aircraft wing-box," in *Proceedings of the 2006 IEEE ICRA Conference*, pp. 701–706, May 2006.